



HAL
open science

Phase transformations and γ' phase stability in model CoAlW superalloys

Ahmad Azzam, A. Hauet, F. Danoix, T. Philippe, Xavier Sauvage, D. Blavette

► **To cite this version:**

Ahmad Azzam, A. Hauet, F. Danoix, T. Philippe, Xavier Sauvage, et al.. Phase transformations and γ' phase stability in model CoAlW superalloys. *Journal of Alloys and Compounds*, 2019, 798, pp.832-845. 10.1016/j.jallcom.2019.05.180 . hal-02156534

HAL Id: hal-02156534

<https://hal.science/hal-02156534>

Submitted on 25 Oct 2021

HAL is a multi-disciplinary open access archive for the deposit and dissemination of scientific research documents, whether they are published or not. The documents may come from teaching and research institutions in France or abroad, or from public or private research centers.

L'archive ouverte pluridisciplinaire **HAL**, est destinée au dépôt et à la diffusion de documents scientifiques de niveau recherche, publiés ou non, émanant des établissements d'enseignement et de recherche français ou étrangers, des laboratoires publics ou privés.



Distributed under a Creative Commons Attribution - NonCommercial 4.0 International License

Phase transformations and γ' phase stability in model CoAlW superalloys

A. Azzam^a, A. Hauet^a, F. Danoix^a, T. Philippe^b, X. Sauvage^a, D. Blavette^a

^aNormandie Université, UNIROUEN, INSA Rouen, CNRS, GPM, 76800 Saint Étienne du Rouvray, France

^bPhysique de la Matière Condensée, Ecole Polytechnique, CNRS, 91128 Palaiseau, France

Abstract

The present work aims at understanding the transformation mechanisms of γ' -L1₂ precipitates in the ternary Co-Al-W system from quenched state to thermodynamic equilibrium. Three alloys with compositions Co-9Al-7W, Co-10Al-12W and Co-7Al-9W (at.%) were aged at 900 °C for 10 h, 200h and 1000h. The microstructure has been characterized by transmission and scanning electron microscopies, and the phase composition was determined using atom probe tomography. Results show that irrespective of the initial supersaturation, the quenched state is already decomposed into $\gamma+\gamma'$. This indicates that even in the Co-7Al-9W alloy that lies in the $\gamma+\text{Co}_3\text{W}$ domain of the phase diagram, γ' phase forms at first, indicating that γ' is a metastable phase. In the two other alloys, during ageing at 900 °C γ' phase dissolves and the equilibrium state is composed of γ , CoAl and Co_3W phases. The γ' phase in the Co-7Al-9W alloy dissolves more rapidly compared to the two other alloys that are in the $\gamma+\gamma'$ metastable domain. The volume fraction of Co_3W phase increases rapidly with ageing time in the Co-7Al-9W alloy. Whereas γ' phase is predominant at short ageing times, it becomes a minor phase after 1000h of ageing, and is replaced mostly by the Co_3W phase. As already observed, the transformation from γ' -L1₂ to Co_3W -D019 phase is taking place through a stacking fault. This mechanism occurs in the three alloys. In addition, a new dissolution mechanism interpreted as destabilization of the γ' phase is evidenced in the Co-9Al-7W. The γ' precipitates tend to split along {111} planes. Transmission electron microscopy investigations show that the dissolution and splitting mechanism of the γ' phase is initiated by stacking faults, that are subsequently wetted by the γ phase.

Key words: Co-Al-W superalloys, γ/γ' microstructure, phase stability, dissolution, splitting

* Corresponding author: azzam_002@hotmail.fr

1. Introduction

The discovery by Sato et al. in 2006 [1] of a L1₂ ordered structure (γ' phase) embedded in a disordered FCC matrix (γ) in Co-Al-W alloys have raised a lot of hope. Indeed, this new generation of cobalt based superalloy consisting of a solid solution matrix strengthened by

L1₂ ordered precipitates, similar to Nickel based superalloys is promising for higher operating temperatures in particular for aircraft turbines [2-6]. Unfortunately, in the Co-Al-W system, the $\gamma + \gamma'$ two phase region [1] is relatively narrow, and moreover it was quickly understood that the γ' phase is probably metastable at 900°C [7-11]. Kobayashi *et al.* [7] assumed that γ' decomposes into Co₃W and CoAl stable phases after aging at 900°C, and proposed a new phase diagram in which the $\gamma + \gamma'$ domain is metastable. However, adding new solutes could stabilize the γ' phase at high temperatures [12-16]. Precise understandings of the ternary system and the mechanisms of phase transformation have already been studied [7,8,17,18]. In particular, Pyckzak *et al.*[17] observed the dissolution of γ' in Co-9Al-XW (X=8,9,11 at.%) after 1000h at 900 °C. As a result, it was concluded that the thermodynamically stable phases could be the solid solution γ , the CoAl B2 phase and the Co₃W D0₁₉ phase, whereas the γ' phase could be only metastable. It is worth mentioning that Co₃W is an incoherent hexagonal ordered phase which is hard to nucleate in the γ matrix, while the coherent γ' phase nucleates easily and could precede the precipitation of the stable Co₃W phase. Such a kinetic pathway is very common in Al base alloys where coherent GP zones precede the precipitation of stable phases [19]. Recently, Li *et al.* [18] explored the L1₂ to D0₁₉ transformation mechanism in Co-Al-W alloys. The stability of γ' phase is not confirmed [19], the role of stacking faults as an intermediate step of L1₂ to D0₁₉ in these alloys was evidenced.

The uncommon behavior of the γ' phase in ternary Co-Al-W alloys remains unclear. This work aims at investigating the microstructural evolution in three different ternary Co-Al-W alloys at 900 °C with various Al, W content, using TEM, SEM and APT. The formation of L1₂ precipitates during cooling, their growth and their possible dissolution in favor of other stable phases after long-time ageing will be discussed. According to the phase diagram (Fig.1), the 7Al9W alloy is located in $\gamma' + \text{Co}_3\text{W}$ region while the others (9Al7W and 10Al112W) are in the two $\gamma + \gamma'$ domain [1]. This paper follows a previous work related to the kinetics of growth of the L1₂ phase in a Co-7Al-9W alloy [20].

2. Experimental methods

Three polycrystalline ingots of ternary Co based alloys with a diameter of 8 mm and 60 mm long were prepared in a vacuum induction melting furnace at the Office National d'Etudes et de Recherches Aéropatiales (ONERA), France. Two target compositions were chosen in the two-phase $\gamma + \gamma'$ field, and a third, poorer in Al, in the two-phase $\gamma + \text{Co}_3\text{W}$ region, near the three-phase $\gamma + \gamma' + \text{Co}_3\text{W}$ domain (Fig.1). After solidification, ingots were subjected to a

homogenisation treatment at 1300°C for two hours under argon atmosphere, followed by water quenching. Samples were subsequently aged at 900°C for 10 h, 200 h and 1000 h under argon atmosphere in a vertical furnace, and then water quenched. To limit possible precipitation of γ' during the quench, all heat treatments were performed on thin samples (thickness 300 μm). The grain size measured by electron backscattered diffraction (EBSD) was about 100 μm .

The as-quenched and annealed microstructures were investigated by scanning electron microscopy (SEM) using a Zeiss Leo 1530 XB microscope equipped with a back-scatter electron (BSE) detector and energy dispersive X-ray spectrometer (EDS). Transmission electron microscopy (TEM) characterizations were done using Jeol 2010 and Jeol ARM 200 F microscopes operated at 200 kV. Samples for SEM were mechanically grounded and then electro-polished in a solution of methanol with 5% perchloric acid, at a temperature of -40 °C and a voltage of 18 V. For TEM analyses, discs of 3mm in diameter were cut and mechanically polished to a thickness less than 100 μm and then thinned to electron transparency in a twin jet polishing system (TenuPol-5) with the same solution and conditions as above. The size distribution and volume fraction of precipitates were determined from SEM and TEM micrographs using ImageJ software.

APT analyses were conducted in voltage mode. Samples for APT were prepared by lift out using focused ion beam (Zeiss Nvision 40 FIB-SEM). Initial annular milling was performed with an accelerating voltage of 30 kV. The final step was carried out with a low voltage (2 kV) to reduce damage caused by the Ga ions. APT experiments were carried out using a local electrode atom probe (LEAP 4000 HR®, Cameca instrument), with a pulse frequency of 200 KHz, a pulse fraction of 20 % of the standing voltage, and a mean detection rate of 0.2 ion/pulse. APT data were treated using IVAS ® 3.6.8 software. All measurements were performed at 80 K.

The average overall compositions of the three investigated alloys are given in Table 1. They were measured in the as-quenched condition by APT and by energy dispersive X-ray spectroscopy (EDS), and result from more than twenty independent analyses in both cases. To simplify the notations the three alloys are hereafter termed as 9Al7W, 7Al9W and 10Al12W respectively. The measured compositions (see Table1) are in reasonable agreement with target compositions. XRD analyses were carried out on a Bruker D8 diffractometer in Bragg-Brentano configuration using Co anti-cathode ($K\alpha_1$ and $K\alpha_2$ rays ($\lambda_1=1.7890 \text{ \AA}$) and ($\lambda_2=1.7928 \text{ \AA}$)). In all the as-quenched alloys, the lattice parameter of γ phase was determined as $0.3580\pm 0.0004 \text{ nm}$. The resolution of the XRD set up did not allow to reveal any significant

lattice mismatch between the 3 alloys. The γ' lattice parameter (deduced from lattice reflections) in 10Al12W after 10 hours annealing at 900°C was 0.3590 ± 0.0004 nm, which corresponds to a 0.3% lattice mismatch with γ' . These values are in accordance with Sato [1] and Pysack [5]. In addition to the γ and γ' phase peaks, weak D0₁₉ peaks have also been identified in 10Al12W after 10 h ageing at 900°C .

3. Experimental results

3.1. As quenched alloy

Globular or lamellar precipitates are found to decorate some of the grain boundaries (Fig.2a) in the 10Al12W. Few globules have also been found in the core of some grains (Fig.2b), they appear essentially white-contrasted in the γ grey matrix, which indicates that they are enriched in W. EDS analyses (data not shown there) made it possible to identify them as Co₃W and occasionally as Co₇W₆. The latter probably result from solidification, and were dissolved during homogenization treatment. Darkly imaged particles which have grown alongside a Co₃W grain (arrowed in Fig.2a) were identified as CoAl. TEM investigations revealed that small precipitates nucleate during quenching in the three alloys (Fig.3a, c and e). They were identified as L1₂ phase precipitates by electron diffraction and this is confirmed by dark field images obtained with a {001} superlattice reflection. The diameter distributions plotted in Fig.3b, d and f show significantly larger precipitates in 9Al7W. At a larger scale, TEM observations also revealed many small stacking faults and dislocations dispersed in the matrix of the 9Al7W alloy (Fig.4a). More extended stacking faults are present in 7Al9W (Fig.4b) with sometimes small embedded platelets identified as Co₃W. In this alloy, electron diffraction shows additional spots (Fig.4c). Dark field images taken from these additional spots revealed groups of small precipitates in γ' depleted zones (Fig.4d and e). The nearest spot from the center corresponds to a lattice spacing of 0.217 nm which corresponds to the interplanar spacing of Co₃W. Globular precipitation of this phase is thought to occur in 7Al9W, and to compete with γ' phase.

Further investigations of the fine scale microstructure and composition were performed using APT. Fig.5 shows the 3D reconstructions of some analyses condition in the quenched alloys. The nanosized γ' precipitates are delineated by a threshold value of 11 at.% W isoconcentration surface (isosurface). The proximity histogram (or proxigram) was then calculated from these isosurfaces and used to quantify the partitioning behavior of solute atoms across the γ/γ' interface. As shown in Fig.5, W (unlike Al) shows a high degree of partitioning in the γ' phase for the three alloys. Interestingly, in the 9Al7W alloy, the

proxigram reveals a depletion zone about 2 nm (Fig.4b) width at the γ/γ' interface. This suggests that the growth of γ' precipitates is limited by the diffusion of W in the γ matrix. This also reflects a local equilibrium state at the interface. The compositions of γ and γ' phases were measured far from interfaces by averaging the concentration values (referred as far-field values) and are summarized in table 2. The standard deviation σ can be written as $\sigma = (C_i(1 - C_i)/N)^{1/2}$ with C_i is the average concentration of element i and N the total number of atoms in the selected γ' precipitates (or in the γ phase) [21].

3.2 Evolution after isothermal annealing for 10 hours at 900°C

As shown in Fig. 6a, the 9Al7W remains perfectly two-phase $\gamma + \gamma'$. However in 7Al9W and 10Al12W, new lamellar or globular Co_3W precipitates were observed along grain boundaries on BSE micrographs. In addition, intergranular regions where lamellar Co_3W have grown at the expense of the surrounding γ' phase, are observed in the 7Al9W. However, because of their small volume fraction, Co_3W intergranular precipitates most probably do not affect significantly the overall composition of the two-phase $\gamma+\gamma'$ regions. The morphological evolution of γ' precipitates is shown in Fig.6. The minimization of the elastic and interaction energies lead to cuboidal γ' precipitates aligned along the elastically soft $\langle 100 \rangle$ directions. Beside, the dark field TEM micrographs reveal small secondary L_{12} precipitates in the γ regions in the 7Al9W alloy (Fig.6c). They are probably formed during quenching from 900°C, and result from the remaining supersaturation in W. For cubic precipitates the equivalent radius R has been defined as half of the cube edge ($R=d/2$). The experimental particle size distributions are generated from TEM micrographs and for the precipitates aligned near the $\langle 100 \rangle$ directions are presented in (Fig.6b and d). In the highly supersaturated 10Al12W alloy, coalescence of neighboring particles is observed in addition to Ostwald ripening. This lead to a final microstructure consisting of squared, rectangular, and L or T shaped particles (Fig.6e). APT analyses were performed on aged alloys. The 3D reconstructions and the related proxigrams of the aged alloys are represented in Fig.7. The average compositions of γ and γ' phases are given in table 3. The volume fraction of γ' phase, $\phi^{\gamma'}$ derived from phase compositions experimentally measured by APT, was calculated using the lever rule:

$$\phi^{\gamma'} = \frac{C_i^0 - C_i^{\gamma}}{C_i^{\gamma'} - C_i^{\gamma}}$$

where C_i^0 is the average bulk composition for element i ($i = \text{Co, Al, W}$) given in table 1, $C_i^{\gamma'}$ and C_i^{γ} are the composition of element i in γ' and γ respectively measured by APT.

3.3. Evolution after isothermal annealing for 200 and 1000 hours at 900 °C

3.3.1. 10Al12W alloy

After 200 h of annealing, the morphology observed by BSE has slightly changed as compared to 10 h. New Co_3W lamellae surrounded by CoAl B2 have developed at some grain boundaries (Fig.8a). In the core of the grains, globular quenched Co_3W precipitates became slightly bigger, and some scarcely dispersed new Co_3W lamellae are visible. The γ' precipitates have the same morphology after 10 h, with a surface fraction of 80% (Fig.8b), in agreement with phase diagram. The cross section of the Co-Al-W phase diagram (Fig.1) shows that this alloy lies in the $\gamma + \gamma'$ region with a high volume fraction of γ' phase (about 80%). However, After 1000 h of annealing (Fig.8b and c), γ' precipitates disappear in certain zones where Co_3W lamellae are only surrounded by the γ phase (Fig.8c). Clearly γ' precipitates are partly dissolved and their W is probably consumed to form the Co_3W phase. However these zones remain quite rare. Bright field TEM micrographs of $\gamma + \gamma'$ regions do not show dislocations and γ/γ' regions remain unchanged.

3.3.2. 7Al9W alloy

According to the Sato phase diagram, the 7Al9W alloy is expected to lie in the two-phase region ($\gamma + \text{Co}_3\text{W}$) very near to the three-phase domain ($\gamma + \gamma' + \text{Co}_3\text{W}$). After 200 h of annealing, we observe some morphological transformations in BSE micrographs. The grain boundaries appear as large γ strips in which Co_3W lamellae and globules are embedded (Fig.9a). Long lamellae are developed in the grain cores, which can reach a few tens of micrometers. The latter cross the $\gamma + \gamma'$ microstructure (Fig.9b). Several families of these lamellae intersect during their growth. TEM highlights large stacking faults extending over the γ and γ' phases which are associated to Co_3W lamellae as well as aligned dislocations (Fig.9c). Among the square or rectangular γ' precipitates, we can also see elongated or egg-shaped precipitates separated by wider spaces. We can also observe precipitates with rounded corners. This suggests a reorientation of the interfaces at the corners which is probably caused by a loss of coherence and a beginning of dissolution of the $L1_2$ phase. After 1000 h of annealing (Fig.9d), the same behavior is observed, resulting in two types of zones: (1) zones

without γ' phase, but only composed of Co_3W lamellae and globules in the γ matrix, (2) more rare zones where the $\gamma + \gamma'$ structure is preserved, with tight square precipitates separated by narrow channels (yellow zoom in Fig.9d). Image analysis revealed a surface fraction of 28 % for Co_3W and 5% for γ' . The composition of γ regions, as provided by EDS analyses, is found to be 8.2 ± 0.2 at.% Al and 5.48 ± 0.37 at.% W. Compared to APT composition values measured after 10 h of annealing (7 at.% Al and 8 at.% W), it can be concluded that γ becomes richer in Al and poorer in W. The transformation $\gamma + \gamma'$ to $\gamma + \text{Co}_3\text{W}$ requires that Al diffuses from γ' towards γ , and W is thought to be rejected from γ and γ' to form the Co_3W phase. In accordance with literature [22,23], the D0_{19} structure grows in the FCC structure with the following crystallographic relations: $(111)_{\text{FCC}} // (0001)_{\text{D0}_{19}}$ and $\langle 112 \rangle_{\text{FCC}} // \langle 1-100 \rangle_{\text{D0}_{19}}$. This was already observed in other Co-Al-W alloys [8,14,18].

3.3.3. 9Al7W alloy

The 9Al7W alloy is expected to be in the $\gamma + \gamma'$ region with a lower γ' volume fraction (around 25%) as compared to 10Al12W. BSE micrographs (Fig.10a and b) show that the microstructure remains mainly two-phase $\gamma + \gamma'$ after 200 h of annealing. It can be noticed that many twins have developed (arrow in Fig.10a). After 1000 h, a small amount of Co_3W has nucleated at the grain boundaries and more rarely in the core of grains (Fig.10c). However, the alloy remains mainly composed of both γ and γ' phases. The γ' precipitates have the shape of aligned cuboids of various sizes (discontinuous rafting) [14,16,24]. Note that regions with wide γ channels are periodically distributed where L1_2 precipitates remain tight (Fig.10d). The width of γ corridors determined from SEM micrographs after 1000 h is double as compared to what it is after 200 h. TEM micrographs (Fig.11a) exhibit a labyrinth structure. As in the 7Al9W alloy, precipitate corners are often rounded and adopting oblong or egg shapes, suggesting the dissolution of γ' phase (Fig.10b). As shown in Fig.11a and b, many precipitates are splitted. The splits are not parallel to (001) as already observed in the Ni based-super alloys [25], but rather along the $\{111\}$ planes (Fig.11c and d). A similar splitting mechanism is observed after 1000 h of annealing (Fig.11e, f and g). The black contrast observed at the particle corners indicates high elastic stress without loss of coherency (Fig.11e and f). The microstructure given in Fig.11e evidences the presence of split lines that can be derived from the stacking faults initially present before splitting (Fig.11e). As shown in Fig.11b, dark field micrographs do not reveal any other phase in the splitted regions. EDS concentration profiles were collected (Fig.12) : Profile 1 (Fig.12a) is related to $\{001\}$ interface, while profile 2 are related (Fig.12a) to splitted corridors formed after annealing. Table 4 gives compositions

derived from the profiles of Fig.11. The concentration profiles do not indicate any segregation at the interfaces and their variations are simply related to γ and γ' phases.

4. Discussion

4.1. As quenched alloys

As in Ni based superalloys, the ordered $L1_2$ γ' precipitates nucleate and grow quickly during quench. However, this $L1_2$ ordered phase is thought to be metastable in Co-based superalloys. Experiments have shown that it partially or completely disappears after long ageing. This is particularly pronounced in the 7Al9W alloy (in the $\gamma + Co_3W$ two-phase domain of the phase diagram), where Co_3W precipitates should be observed in this case. In contrast, the γ' phase is the major phase after quenching during the early stages of ageing at 900°C. The stable Co_3W phase then nucleates and grows at the expense of the metastable γ' phase that gradually dissolves. For higher solute content (10Al12W), intergranular and intragranular globular Co_3W are able to nucleate and grow during quenching. Small stacking faults and dislocations present in the alloy after quenching can be considered as suitable sites for nucleation of Co_3W and CoAl.

4.2. Evolution after isothermal annealing for 10 hours at 900°C

Let us now switch to the kinetics evolution of the microstructure. A large part of nucleation of the γ' phase occurs during quench, so that mostly growth is observed in the early stages of ageing at 900°C. Coarsening of the γ' phase is then rapidly observed [20]. Let us remember that coarsening is driven by the decrease of the interfacial energy. The microstructural evolution of the material is also strongly affected by the coherency elastic field due to γ/γ' lattice mismatch. The γ' particles are found first roughly near relatively spherical; then they get square or rectangular shaped. Subsequently, as they create long-range elastic strain fields, they become spatially correlated, and aligned along soft $\langle 001 \rangle$ directions [26-31]. It is worth mentioning that in the two Al rich alloys (9Al7W and 10Al12W) located in the $\gamma+\gamma'$ metastable domain, the composition of γ and γ' phases are similar to that predicted by the Sato's phase diagram. In addition, the solute contents in γ' are comparable (Table 2). Conversely, in the low Al-content 7Al9W alloy, where Co_3W is expected to be the precipitated phase, the composition of γ' phase remains far from the Sato equilibrium composition, and the decomposition has already partially proceeded after 10h. In the 3 alloys, the stoichiometry $Co_3(Al+W)$ is fairly well respected in γ' (table 3).

4.3. Evolution after isothermal annealing for 200 and 1000 hours at 900°C

In agreement with other authors [8,18], we observed a partial decomposition of γ' in favor of γ and Co_3W and more rarely in favor of the B2-ordered CoAl phase after long term ageing at grain boundaries. The precipitation of this later phase obviously depends on the Al and W contents. The CoAl phase can be accurately spotted by BSE imaging and it was observed to nucleate on Co_3W lamellae in the high W content 10Al12W alloy only. The equilibrium molar fractions as deduced from Kobayashi phase diagram are 12% for 10Al12W and 3% for 9Al7W. Therefore this phase is expected to be minority, even in the 10Al12W only a small fraction is observed at grain boundaries. In the 9Al7W CoAl precipitates are not yet visible. The equilibrium molar fractions derived from Kobayashi phase diagram and the experimental molar fractions of phases are superimposed in Fig.13. The surface fraction (close to volume fraction) of γ , γ' and Co_3W phases were calculated by image analysis for longer aging time (1000 h). Dissolution of the γ' metastable phase is more rapid in the low Al-content 7Al9W alloy and equilibrium towards the $\gamma+\text{Co}_3\text{W}$ state is more quickly reached. This is expected as this alloy is located in the $\gamma+\text{Co}_3\text{W}$ domain.

As compared to Kobayashi phase diagram, the two other higher Al content alloys exhibit some remaining γ' and consequently a lower volume fraction of Co_3W , showing that equilibrium is not reached even after long ageing times. In the three alloys, the nucleation of the incoherent Co_3W phase first occurs at grain boundaries, and growth develops upon annealing. This is expected as GBs are short-circuits for diffusion, and are also favorable sites for heterogeneous nucleation of incoherent phases. The intra-granular transformations are more difficult to understand. Several questions arise: how to explain (1) the partial transformation [14] of γ' into $\text{Co}_3\text{W} + \gamma$ that apparently does not affect the surrounding $\gamma + \gamma'$ regions, (2) the microstructure heterogeneities observed in the $\gamma + \gamma'$ regions in 7Al9W and 9Al7W, (3) the mechanisms leading to the equilibrium?

Let us first consider the two-phase $\gamma + \gamma'$ regions. γ' precipitates are coherent with the matrix and long-range elastic strain fields lead to strong spatial correlation between particles. After prolonged ageing, the aligned square particles produce rafted or labyrinth-like structures. These microstructures are well-known in Ni-based superalloys. More recently they were observed in quaternary Co based superalloys subjected to several thousands hours of annealing [12,13,16]. In these superalloys, where no Co_3W is formed, the following question remains: is there reorganization of the morphology due to elastic strains? This requires the shift of precipitates, the dissolution of those in less favorable sites in favor of the coarsening

of more stable particles (models were developed to describe these processes of coarsening [24,32,33]). Alternatively, is there dissolution of γ' ? In this context, the published studies of L_{12} dissolution by reversion in Ni-based superalloys can be useful to highlight the behavior of Co-Al-W alloys [34-36]. Grosdidier *et al.* underlined the following mechanisms to reduce the elastic energy: (1) local redistribution of solute atoms. (2) Loss of coherency by dislocation pinning at the matrix/precipitates interface. Indeed, during annealing, dislocations are able to move from defects or subboundaries and be trapped by interfaces. (3) Changes in shapes and arrangements of the particles that can move, align themselves, disappear, coagulate with other precipitates, form rafts or labyrinths. It has been shown that during reversion heat treatment, dissolution of the γ' phase does not lead to a continuous and uniform dissolution of γ' precipitates. Because the latter are linked by elastic interactions, dissolution progresses by the successive disappearance of precipitate groups becoming unstable with regard to other groups. The same authors noted that dissolution is also achieved by the fragmentation of large precipitates along $\{100\}$ planes.

Lass [8] recently observed long annealing effects in Co-Al-W alloys at 900°C. He insisted on the low driving force for γ' dissolution and on the coherency effects which could explain that fine coherent precipitates could constitute zones which could remain in a metastable state during long time, without correlation with more distant zones. This corresponds to the previous assessments and involves negligible effects of long range diffusion. Li et al [18] have recently proposed a new model explaining the γ' dissolution into γ and Co_3W . The mechanism, leading to the transformation of L_{12} phase to the D_{019} structure, is well-known [22,23]. This transformation, which is activated by sliding of dense planes, needs first a superlattice intrinsic stacking fault (SISF). The gliding system is $a/3\langle 112 \rangle\{111\}$; $1/3\langle 112 \rangle$ partial dislocations slide along $\{111\}$ planes of the L_{12} phase, and initiate the D_{019} arrangement. At the same time, this process requires long range diffusion of W from L_{12} precipitates to the FCC solid solution and to the new Co_3W phase that needs more W and less Al compared to L_{12} phase. Once initiated, the transformation progress very quickly. Four families of Co_3W lamellae grow on the 4 variants of $\{111\}$ plane family of the FCC lattice, until they are blocked when crossing another family.

Clearly this is the mechanism which allows the formation of the Co_3W phase. It is well observed in the three alloys. This is a local fast process which extends more or less. After 200h of ageing, it is well developed in the 7Al9W alloy, while it is only in the early stage in the two other alloys. This transformation is controlled by several factors such as the stacking fault energy (SFE) of the alloy, the driving force for dissolution related to the composition of

γ' , and the dislocation ability for sliding in γ corridors before being trapped in γ' particles. It was shown recently by computational thermodynamic approach [38] that in Co-Al-W alloys, the SFE decreases with decreasing Al content and increasing W content. The SFE is then potentially lowest in 7Al9W where Co_3W is quickly observed, which could promote the periodic stacking faults formation required for Co_3W growth as well as their extension.

However other dissolution processes are thought to be activated here. Indeed in 7Al9W and 9Al7W, structures similar to those observed during reversion in Ni-based superalloys, are observed. Precipitates elongated or egg shaped, whose facets never seem planar and whose corners are rounded, suggest a dissolution process. Let us recall that corners of precipitates where the curvature is larger, lead to pronounced Gibbs-Thomson capillarity effects that in turn gives rise to a Gibbs energy excess that drives local dissolution in these regions. The non-homogeneous microstructure, where squared and tight precipitates coexist with more rounded particles separated by wide channels and zones without γ' , suggests a reorganization of the $\gamma + \gamma'$ microstructure accompanied by partial dissolution of γ' .

γ' fragmentations along $\{111\}$ planes was observed in 9Al7W . They are thought to occur along stacking faults which are subsequently wetted by the γ phase unless Co_3W form. A similar behavior was highlighted in a CoNi-base superalloy under creep tests [39] where the splitting of the γ' precipitates is interpreted as “wetting” by the disordered γ phase. Fragmentations were also observed during reversion tests in Ni base superalloys by Lee and Grosdidier [34,35,36], who assumed that some precipitates form during quench, and fragmentations result from a loss of coherency. However, these precipitates presented outgrowths at their surface and are always associated with a dislocation networks at the interface. This is not observed here, and we think that the fragmentation is rather an ageing effect. As L_{12} locally dissolves, W atoms have to be rejected into the γ matrix. During long time ageing, rejected W atoms will probably be consumed in new Co_3W lamellae.

These dissolution processes are not observed in 10Al12W where the volume fraction of γ' remains very high, and the microstructure fairly stable. The Co_3W phase transformation is probably delayed because the 3 factors referred above are unfavorable. However it occurred in some scarce zones and probably will continue for longer ageing time. Moreover as CoAl forms, γ' has to dissolve, so that to tend towards the γ -CoAl- Co_3W three-phase equilibrium state.

Finally , in the three alloys, the size of regions where γ' precipitates dissolve at benefit of Co_3W are expected to be of the same order of magnitude of the mean diffusion length for W (

$\sqrt{D_W t}$, D_W is the interdiffusion coefficient of W in the fcc matrix), which is a few micrometers for an annealing of 1000 h at 900 °C. This is the case for regions located around Co_3W precipitates in Fig.8c, Fig. 9a and Fig. 10.c. Therefore we can anticipate that if the mean distance between Co_3W precipitates is of the same order of $\sqrt{D_W t}$, γ' dissolution could have been potentially complete. As a consequence, regions containing γ' precipitates that do not see, in terms of diffusion, any Co_3W phase remain unaffected and no dissolution is expected. This is confirmed experimentally (see Fig. 8a, 8c and 10.c). However some regions are seen to be unaffected despite they are near Co_3W lamella, such as in Fig. 9d; probably because of the long driving force for dissolution resulting from coherency effects, as suggested by Lass *et al.* [8]

5. Summary

1. Electron microscopy, X ray and APT experiments conducted on the ageing behavior of three families of model Co-Al-W superalloys at 900°C clearly demonstrate that γ' is a metastable phase at 900°C. This phase nucleates during quenching from 1300°C. After long time ageing, the $\gamma + \gamma'$ structure transforms into the expected $\gamma + \text{Co}_3\text{W}$ equilibrium state in 7Al9W, and into the $\gamma + \text{Co}_3\text{W} + \text{CoAl}$ three-phase state in the two other alloys that are richer in Al, an element that is essential for the precipitation of the Al-rich CoAl phase.
2. This transformation is already initiated during quench. Depending on Al and W contents, small globular Co_3W can form at the grain boundaries or be dispersed in the grain interior. Near the binary $\gamma + \text{Co}_3\text{W}$ region of the phase diagram, a fine precipitation of Co_3W can compete with γ' precipitation.
3. The γ' phase transformation is almost complete after 200h ageing in 9Al7W; it only begins in the two other alloys. A slow process of dissolution by surface erosion and fragmentation, and a fast process proceeding from a stacking fault, are highlighted. Depending on the Al and W contents, three reasons could favor the transformation: low SFE, high driving force for dissolution, and ability of dislocations for gliding in the γ channels.
4. Dissolution occurring through the fragmentation of γ' precipitates and underlying the role of stacking faults, is predominant in the 9Al7W.
5. The diffusion-controlled dissolution of γ' at benefit of Co_3W (mostly globular but not only) is found in good agreement with the diffusion length of W. In other γ/γ' regions near Co_3W (mostly lamellar), the transformation is blocked and unaffected by dissolution, probably due to coherency effect.

As a conclusion, the metastability of γ' that is here proved. This is of utmost importance both from a fundamental point of view and for implementation in high temperature applications. In the three alloys, the mechanism of intra-granular formation of the Co_3W phase from both γ and γ' phase has been discussed in details with regards to the importance of (111) stacking faults role.

Acknowledgments

Authors wish to thank Didier Locq and Pierre Caron (ONERA) for fruitful discussions and for supplying samples.

Bibliography

- [1] J. Sato, T. Omori, K. Oikawa, I. Ohnuma, R. Kainuma, K. Ishida, 2006. Cobalt-Base High-Temperature Alloys, *Science* 312 (2006) 90–91
- [2] A. Suzuki, T.M. Pollock, High-temperature strength and deformation of γ/γ' two-phase Co-Al-W-base alloys, *Acta Mater.* 56 (2008) 1288-1297.
- [3] Y.-J. Wang, C.-Y. Wang, A comparison of the ideal strength between $\text{L}_{12}\text{Co}_3(\text{Al},\text{W})$ and Ni_3Al under tension and shear from first-principles calculations, *Appl. Phys. Lett.* 94 (2009) 261909.
- [4] A. Bauer, S. Neumeier, F. Pyczak, R.F. Singer, M. Göken, Creep properties of different γ' -strengthened Co-base superalloys, *Mater. Sci. Eng., A* 550 (2012) 333-341.
- [5] F. Pyczak, A. Bauer, M. Göken, S. Neumeier, U. Lorenz, M. Oehring, N.Schell, A. Schreyer, A. Stark, F. Symanzik, Plastic deformation mechanisms in a crept L_{12} hardened Co-base superalloy, *Mater. Sci. Eng., A* 571 (2013) 13-18.
- [6] L. Shi, J.J. Yu, C.Y. Cui, X.F. Sun, The creep deformation behavior of a single crystal Co-Al-W-base superalloy at 900°C, *Mater. Sci. Eng., A* 635 (2015) 50-58.
- [7] S. Kobayashi, Y. Tsukamoto, T. Takasugi, H. Chinen, T. Omori, K. Ishida, S. Zaefferer, Determination of phase equilibria in the Co-rich Co-Al-W ternary system with a diffusion-couple technique, *Intermetallics* 17 (2009) 1085-1089.
- [8] E. A. Lass, M. E. Williams, C. E. Campbell, K.-W. Moon, U. R. Kattner, γ' Phase Stability and Phase Equilibrium in Ternary Co-Al-W at 900 °C, *J. Phase Equilib. Diffus.* 35 (2014) 711-723.

- [9] Y. Tsukamoto, S. Kobayashi, T. Takasugi, The stability of γ' -Co₃(Al, W) phase in Co-Al-W ternary system, *Mater. Sci. Forum* 654 (2010) 448-451.
- [10] C. Jiang, First-principles study of Co₃(Al, W) alloys using special quasi-random structures, *Scripta Mater.* 59 (2008) 1075-1078.
- [11] J.E. Saal, C. Wolverton, Thermodynamic stability of Co-Al-W L₁₂ γ' , *Acta Mater.* 61 (2013) 2330-2338.
- [12] F. Xue, H.J. Zhou, X.F. Ding, M.L. Wang, Q. Feng, Improved high temperature γ' stability of Co-Al-W-base alloys containing Ti and Ta, *Mat. Letters*, 112 (2013) 215-218.
- [13] S. Kobayashi, Y. Tsukamoto, T. Takasugi, Phase equilibria in the Co-rich Co-Al-W-Ti quaternary system, *Intermetallics* 19 (2011) 1908-1912.
- [14] D. J. Sauza, P. J. Bocchini, D. C. Dunand, D. N. Seidman, Influence of ruthenium on microstructural evolution in a model Co-Al-W superalloy, *Acta Mater.* 117 (2016) 135-145.
- [15] I. Povstugar, P.-P. Choi, S. Neumeier, A. Bauer, C.H. Zenk, M. Göken, D. Raabe, Elemental partitioning and mechanical properties of Ti- and Ta-containing Co-Al-W-base superalloys studied by atom probe tomography and nanoindentation, *Acta Mater.* 78 (2014) 78.
- [16] V.A. Vorontsov, J.S. Barnard, K.M. Rahman, H.-Y. Yan, P.A. Midgley, D. Dye, Coarsening behaviour and interfacial structure of γ' precipitates in Co-Al-W based superalloys, *Acta Mater.* 120 (2016) 14-23.
- [17] F. Pyczak, A. Bauer, M. Göken, et al., The effect of tungsten content on the properties of L12-hardened Co-Al-W alloys, *J. Alloy. Compd.* 632 (2015) 110-115.
- [18] Y. Li, F. Pyczak, M. Oehring, et al., Thermal stability of γ' phase in long-term aged Co-Al-W alloys, *J. Alloy. Compd.* 729 (2017) 266-276.
- [19] A. Bigot, F. Danoix, P. Auger, D. Blavette, A. Menand, 3D reconstruction and analysis of GP zones in Al-1.7Cu (at.%): a tomographic atom probe investigation, *Appl. Surf. Sci.* 94-95 (1996) 261-266.
- [20] A. Azzam, T. Philippe, A. Hauet, F. Danoix, D. Locq, P. Caron, D. Blavette, Kinetics pathway of precipitation in model Co-Al-W superalloy, *Acta Mater.* 145 (2018) 377-387.
- [21] F. Danoix, G. Grancher, A. Bostel, D. Blavette, Standard deviations of composition measurements in atom probe analyses—Part II: 3D atom probe Ultramicroscopy, 107 (2007) 739-743.
- [22] P.A. Carvalho, P.M. Bronsveld, B.J. Kooi, J.Th.M. De Hosson, On the fcc→D019 transformation in Co-W alloys, *Acta Materialia* 50 (2002) 4511–4526.

- [23] Q. Z. Chen, A. H. W. Ngan, B. J. Duggan, The $L1_2 \leftrightarrow DO19$ transformation in the intermetallic compound Fe_3Ge , *J. of Materials Science* 33 (1998) 5405 – 5414.
- [24] Y. Wang, D. Banerjee, C.C. Su, A.G. Khachaturyan, Field kinetic model and computer simulation of precipitation of $L1_2$ ordered intermetallics from f.c.c. solid solution, *Acta Mater.* 46 (1998) 2893-3001.
- [25] M. Doi, T. Miyazaki, T. Wakatsuki, The effect of elastic interaction energy on the morphology of γ' precipitates in Nickel-based alloys, *Materials Science and Engineering*, 67 (1984) 247-258.
- [26] T. Miyazaki, H. Imamura, H. Mori, T. Kozakal, Theoretical and experimental investigations on elastic interactions between γ' -precipitates in a Ni-Al alloy, *J Mater Sci* 16 (1981) 1197-1203.
- [27] M. Doi, T. Miyazaki, γ' Precipitate morphology formed under the influence of elastic interaction energies in nickel-base alloys, *Materials Science and Engineering* 78 (1986) 87-94.
- [28] A. D. Sequeira, H. A. Calderon, G. Kostorz, Shape and growth anomalies of γ' precipitates in Ni-Al-Mo alloys induced by elastic interaction, *Scripta Metallurgica et Materialia* 30 (1994) 7-12.
- [29] Y. Wang, D. Banerjee, C. C. Su, A. G. Khachaturyan, Field kinetic model and computer simulation of precipitation of $L1_2$ ordered intermetallics from f.c.c. solid solution, *Acta Materialia* 46 (1998) 2983-3001.
- [30] V. Vaithyanathan, L. Q. Chen, Coarsening of ordered intermetallic precipitates with coherency stress, *Acta Materialia* 50 (2002) 4061-4073.
- [31] Y. Tsukada, Y. Murata, T. Koyama, M. Morinaga, Phase-Field Simulation of the Effect of Elastic Inhomogeneity on Microstructure Evolution in Ni-Based Superalloys, *Materials Transactions* 50 (2009) 744-748.
- [32] K. Thornton, N. Akaiwa, P.W. Voothees, Large-scale simulations of Ostwald ripening in elastically stressed solids. II. Coarsening and particle size distribution, *Acta Materialia*, 52 (2004) 1365-1378.
- [33] V. Vaithyanathan, L.Q. Chen, Coarsening of ordered intermetallic precipitates with coherency stress, *Acta Materialia*, 50 (2002) 4061-4073.
- [34] T. Grosdidier, A. Hazotte, A. Simon, Precipitation and dissolution processes in γ/γ' single crystal nickel-based superalloys, *Materials Science and Engineering A* 256 (1998) 183–196.
- [35] T. Grosdidier, A. Hazotte, A. Simon, On the dissolution mechanisms of γ' precipitates in nickel-based superalloys, *Scripta Metallurgica et Materialia*, 30, 10 (1994) 1257-1262.

- [36] H. T. Lee, S. W. Lee, The morphology and formation of gamma prime in nickel-base superalloy, *Journal of materials science letters*, 9 (1990) 516-517.
- [37] M. Doi and T. Miyazaki, γ' Precipitate Morphology Formed under the Influence of Elastic Interaction Energies in Nickel-base Alloys, *Materials Science and Engineering*, 78 (1986) 87-94.
- [38] T. L. Achmad, W. Fu, H. Chen et al. Computational thermodynamic and first-principles calculation of stacking fault energy on ternary Co-based alloys, *Computational Materials Science* 143 (2018) 112–117.
- [39] Y.M. Eggeler, J. Müller, M.S. Titus et al., Planar defect formation in the γ' phase during high temperature creep in single crystal CoNi-base superalloys, *Acta Materialia*, 113 (2016) 335-349.

Table 1: The target and measured compositions (in at.%) of the three alloys investigated in this study.

Alloys	EDS measurements (at.%)		APT measurements (at.%)	
	Al	W	Al	W
9Al7W	9.3±0.4	7.4±0.2	10.16±0.09	7.88±0.10
7Al9W	6.9±0.7	10.0±0.8	7.42±0.08	9.69±0.10
10Al12W	9.25±0.77	11.89±0.22	10.64±0.03	12.22±0.20

Table 2: Composition of γ and γ' phases measured from APT in quenched state.

	7Al9W		9Al7W		10Al12W	
	γ	γ'	γ	γ'	γ	γ'
Al (at.%)	7.4±0.10	7.42±0.10	10.57±0.09	10.85±0.18	10.50±0.08	11.05±0.08
W (at.%)	8.45±0.20	15.80±0.22	7.54±0.09	17.04±0.18	9.77±0.08	14.60±0.07

Table 3: Composition of γ and γ' phases measured from APT and the corresponding γ' volume fraction $\phi_{\gamma'}$ and γ' precipitate size (mean radius $\langle R \rangle$) of after ageing for 10 h at 900 °C

	7Al9W		9Al7W		10Al12W	
	Al (at.%)	W (at.%)	Al (at.%)	W (at.%)	Al (at.%)	W (at.%)
Al (at.%)	7.09 ±0.16	8.8±0.17	9.50 ±0.29	10.50±0.38	9.9±0.27	10.86±0.21
W (at.%)	7.67±0.16	16.2±0.15	5.80±0.30	13.9±0.36	5.65±0.28	13.63±0.20
$\phi_{\gamma'} (%)$	29		25		80	
$\langle R \rangle (nm)$	30		29			

Table 4: Composition of W determined from EDS line scanning profiles in 9Al7W alloy ageing at 900°C for 200 h. Profiles 1 and 2 are showed in figure 12.

Alloys	Profile 1	Profile 2
W composition in γ channels (at.%)	6.20±0.84	6.75±0.85
W composition in γ' (at.%)	12.75±1.10	12.84±1.08

Figures

Fig. 1. Isothermal section diagram of the CoAlW ternary system at 900 °C redrawn from Kobayashi et al.[7].

Fig. 2. (a,b,c) microstructure of the 10Al12W quenched alloy : (a and c) Backscattered SEM micrographs showing nucleation of Co₃W at grain boundaries and rarely the CoAl phase heterogeneously nucleated on Co₃W phase (arrowed in (c)) ; (b) bright field TEM micrograph showing globular phases identified as Co₃W by chemical analysis.

Fig. 3. Dark field TEM micrographs (a,c,e) of the quenched alloys (from (010) reflections) and the corresponding precipitate size distributions (b,d,f) : (a,b) 9Al7W ; (c,d) 7Al9W ; (e,f) 10Al12W alloys. Fitted curves (solid lines) are plotted to evaluate the mean precipitate size.

Fig. 4. (a) and (b) Typical bright field TEM micrographs showing stacking faults in 9Al7W and 7Al9W alloys, (c) diffraction pattern along the [211] zone axis showing the presence of additional diffraction spots, (d) dark field TEM micrograph recorded from additional spot, and (e) dark field recorded from a {0-11} superlattice reflection.

Fig. 5. (a,c,e) APT reconstructions of volumes analyzed in the quenched alloys : (a) 7Al9W ; (c) 9Al7W; (e) 10Al12W . The γ' precipitates are highlighted by 12 at.% W isoconcentration surface. (b,d,f) corresponding proxigrams of 12 at.% isosurfaces showing the mean composition of γ and γ' phases: (b) 7Al9W; (d) 9Al7W; (f) 10Al12W.

Fig. 6. (a,c,e) γ/γ' microstructure (TEM dark field images obtained with the (001) γ' reflexion) after ageing at 900 °C for 10 hr: (a) 9Al7W; (c) 7Al9W; (e) 10Al12W alloy. (a) and (c) are dark field TEM micrographs and (e) bright field micrograph. (b,d) experimental particle size distributions : (b) 9Al7W; (d) 7Al9W. Fitted curves (solid line) are plotted to evaluate the mean precipitate size. The white contrast in (e) is due to preferential etching of the γ phase during TEM specimen preparation.

Fig. 7. (a,c,e) APT reconstructions related to aged alloys at 900 °C for 10 hr, showing γ' precipitates delineated with a 11 at.% W isosurface and the corresponding proxigrams (b,d,f) through γ/γ' interfaces : (a,b) 9Al7W; (b,c) 7Al9W ; (c,d) 10Al12W.

Fig. 8. (a,b,c) SEM micrographs showing the microstructural evolution of the 10Al12W alloy after ageing at 900 °C for: (a,b) 200 h , (c,d) 1000 h. (a),(b),(c) are backscattered SEM micrographs and (d) bright field TEM micrograph.

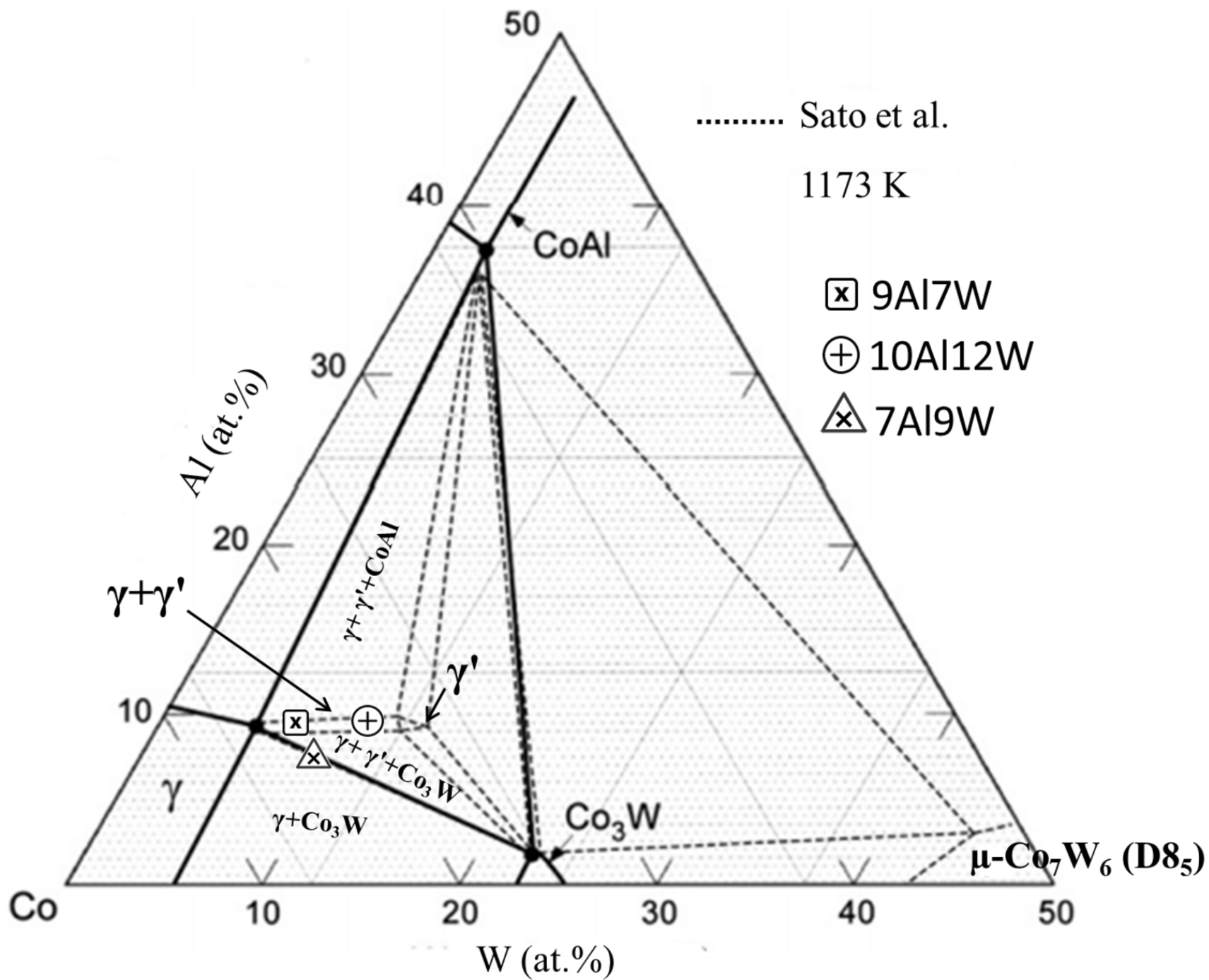
Fig. 9. Microstructural evolution of the 7Al9W alloy after ageing at 900 °C for : (a,b,c) 200h ; (d) 1000 h. (a),(b) and (d) are backscattered SEM micrographs and (c) bright field TEM micrograph. Some dislocation lines were observed in (c) (see dotted arrow).

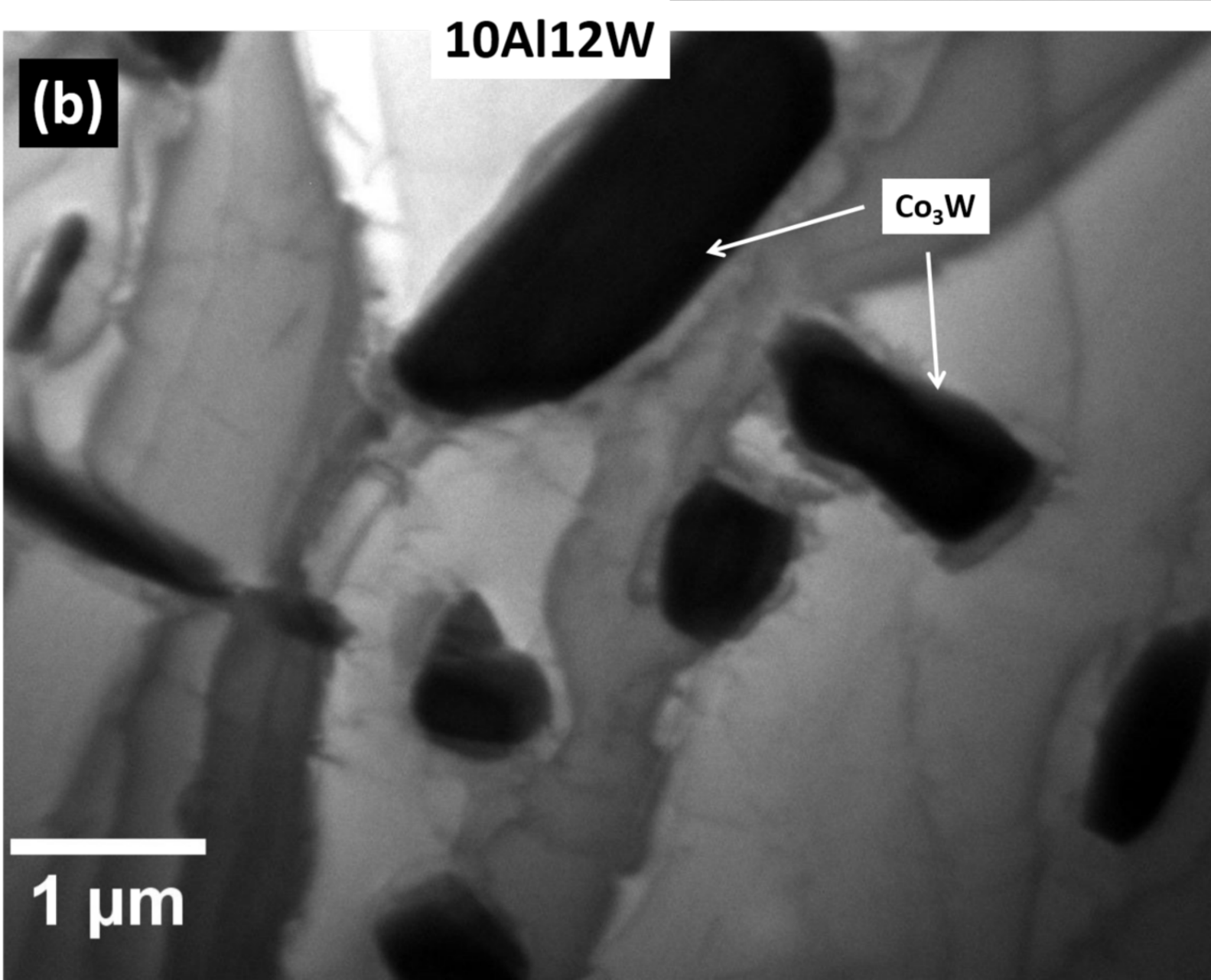
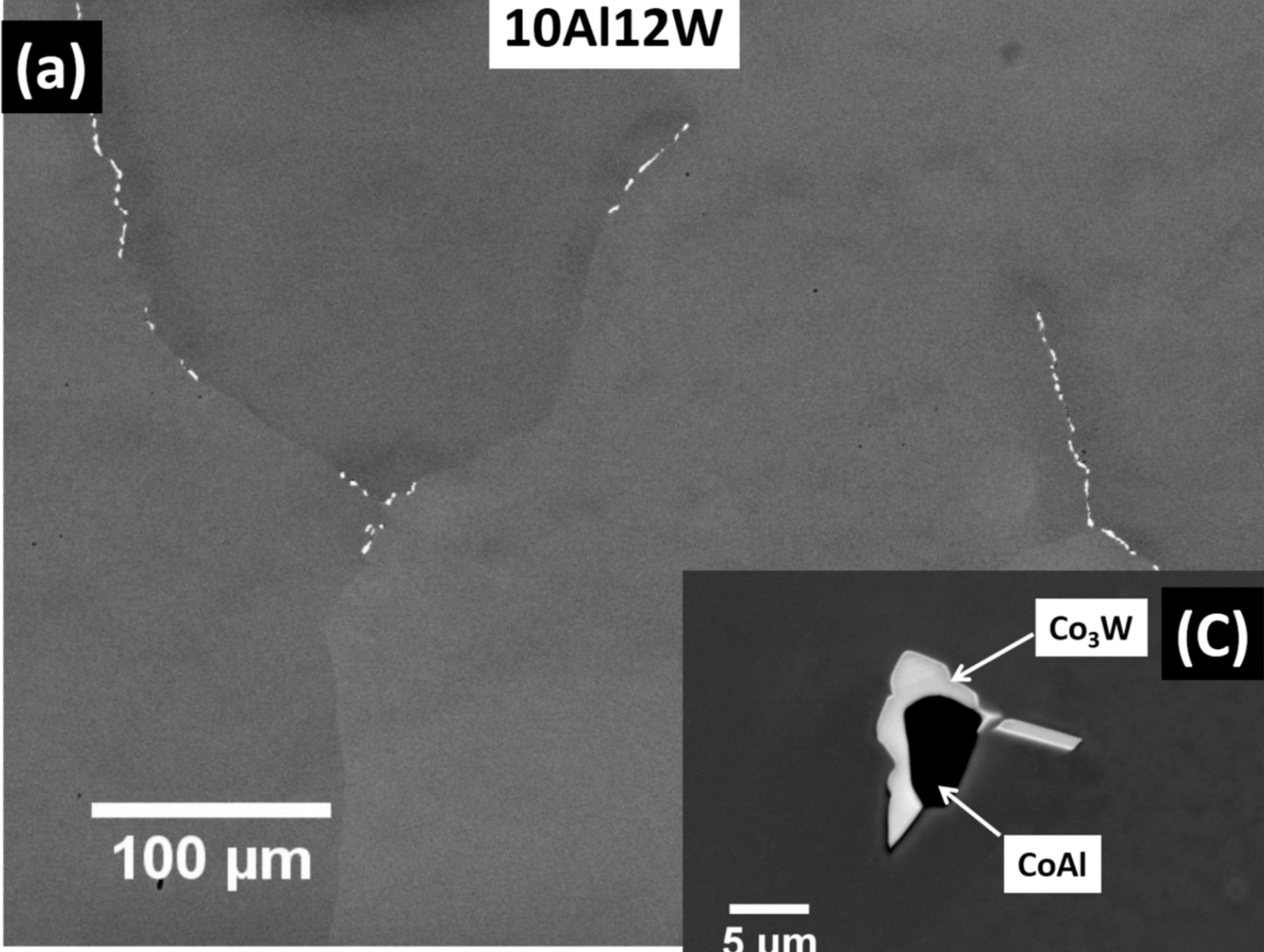
Fig. 10. (a,b,c,d) Backscattered SEM micrographs showing the microstructural evolution of the 9Al7W alloy after ageing at 900°C for : (a,b) 200 h and (c,d) 1000 h.

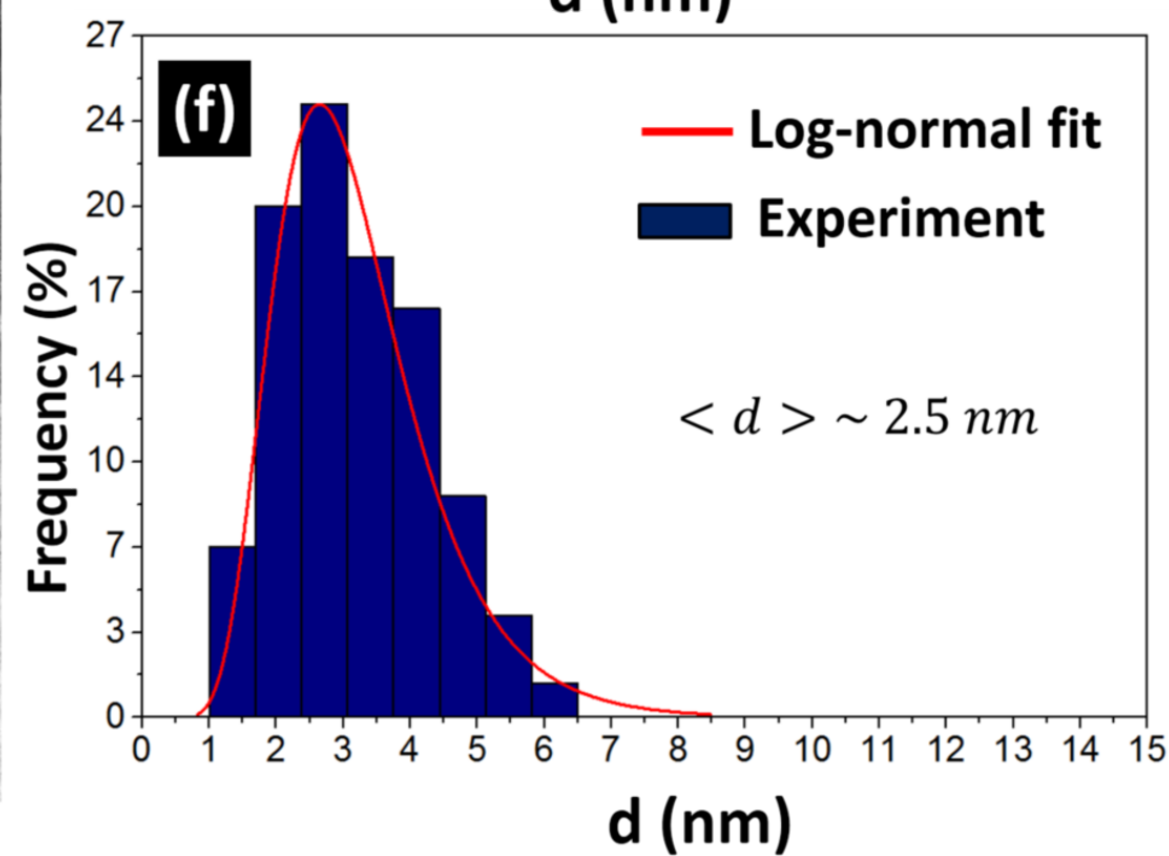
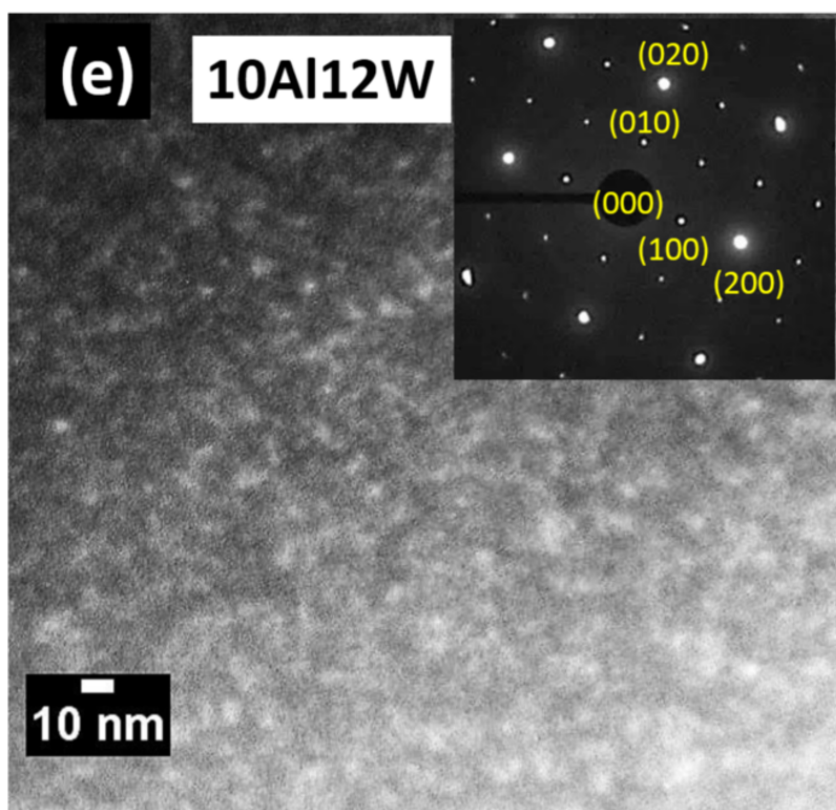
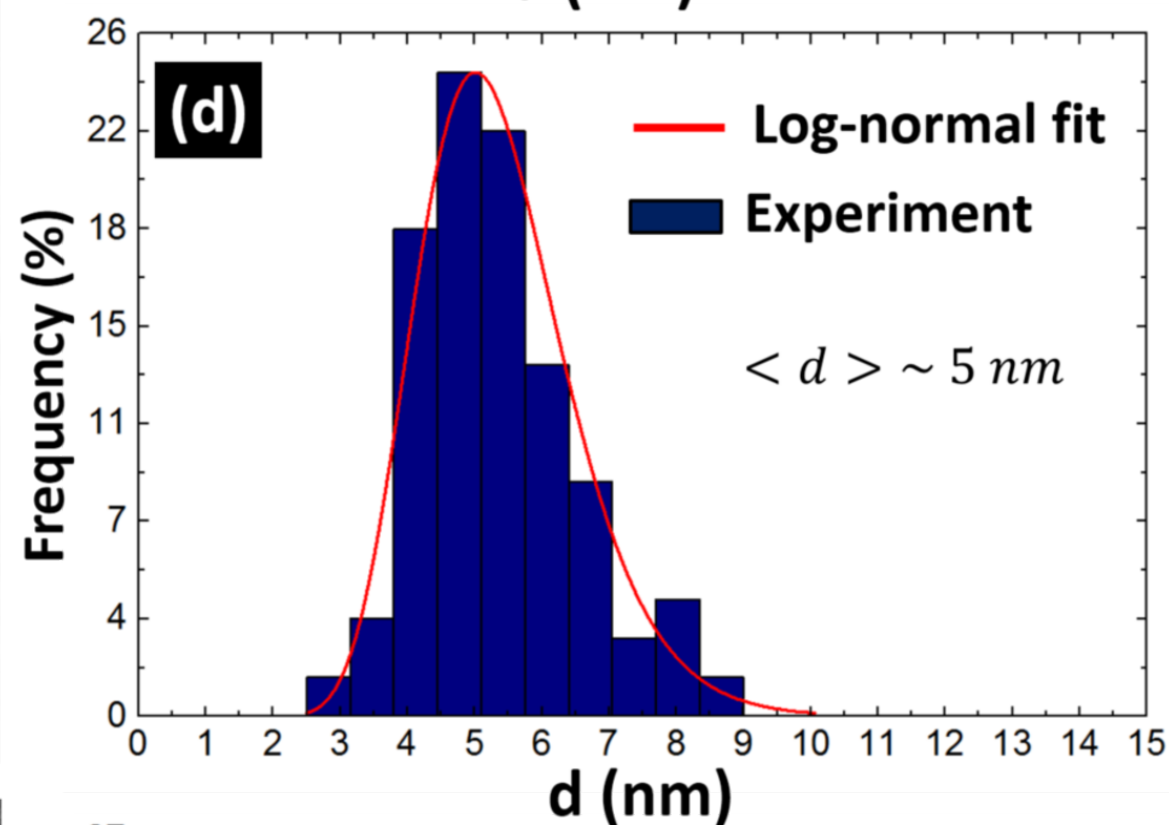
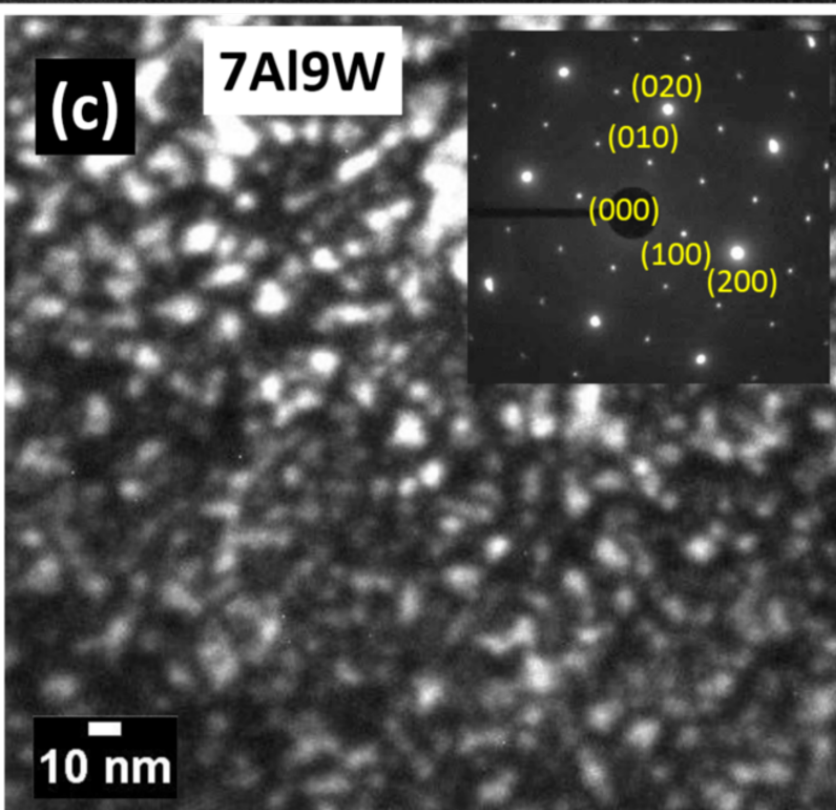
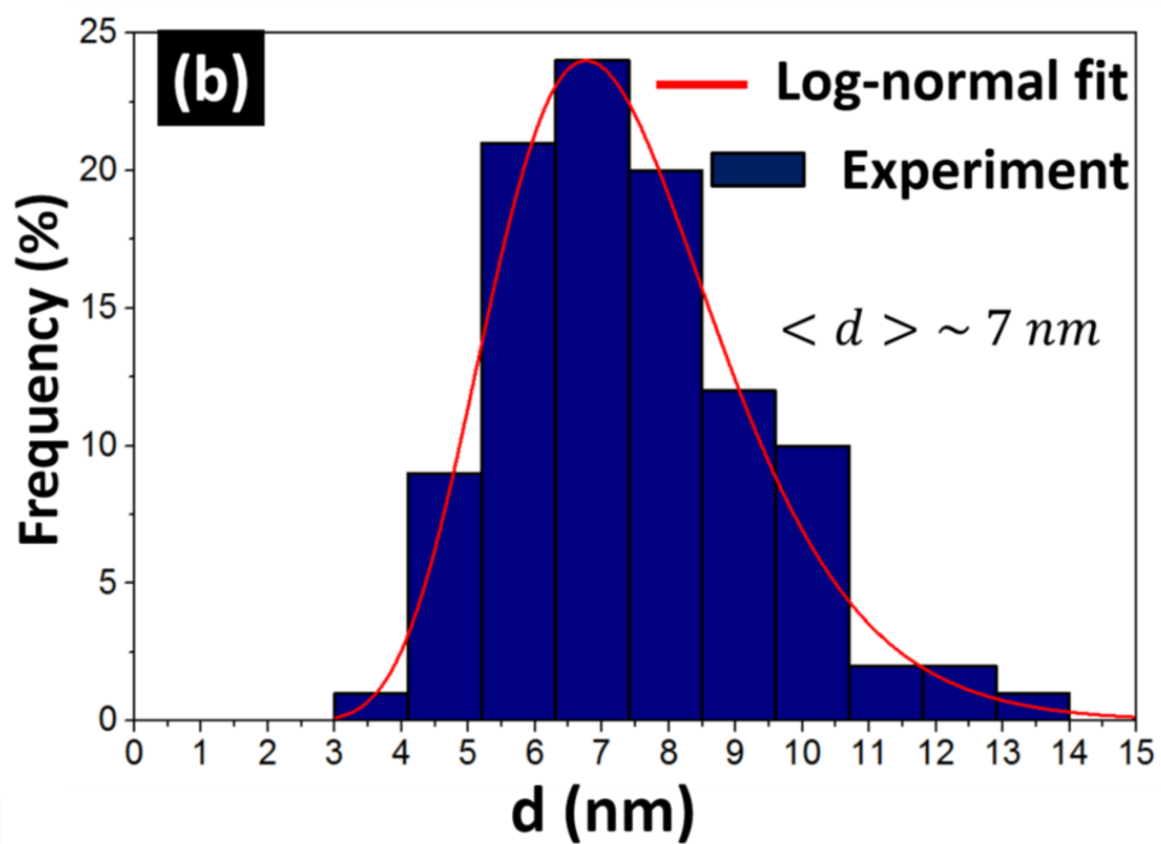
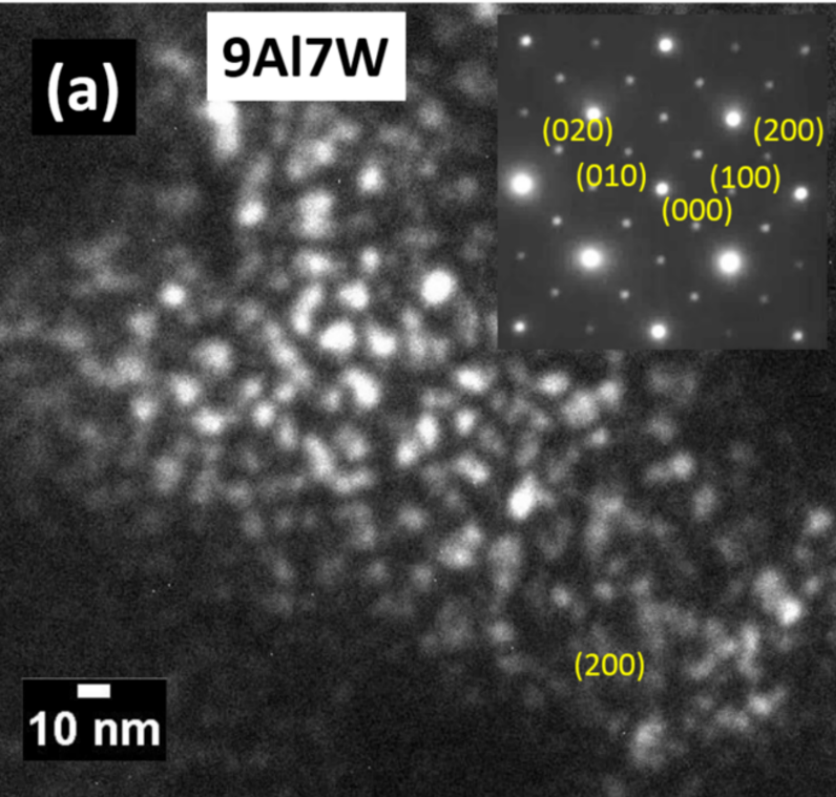
Fig. 11. (a,b) microstructure of the 9Al7W alloy after ageing at 900 °C for 200 h, (a) Bright field TEM micrograph showing a labyrinth microstructure and (b) dark field TEM micrographs showing the splitting of γ' precipitates and their morphological changes during ageing, (c) diffraction pattern along the $\langle 110 \rangle$ zone axis corresponding to (d), (d) bright field TEM micrograph showing the splitting along the $\{111\}$ close packed planes. (e) Bright field TEM micrograph along the $\langle 211 \rangle$ zone axis showing microstructure after ageing for 1000 h. The black contrast observed at the particle corners indicates high elastic stresses (see yellow dotted arrow). Stacking fault contrast is also observed (see black dotted arrow). (f) and (g) are bright and dark field TEM micrographs along the $\langle 211 \rangle$ zone axis showing the same splitting mechanism along the $\{111\}$ planes.

Fig. 12. (a) HAADF micrograph of the 9Al7W alloy after ageing at 900 °C for 200 hr, (b) corresponding EDS W and Al line scan profiles.

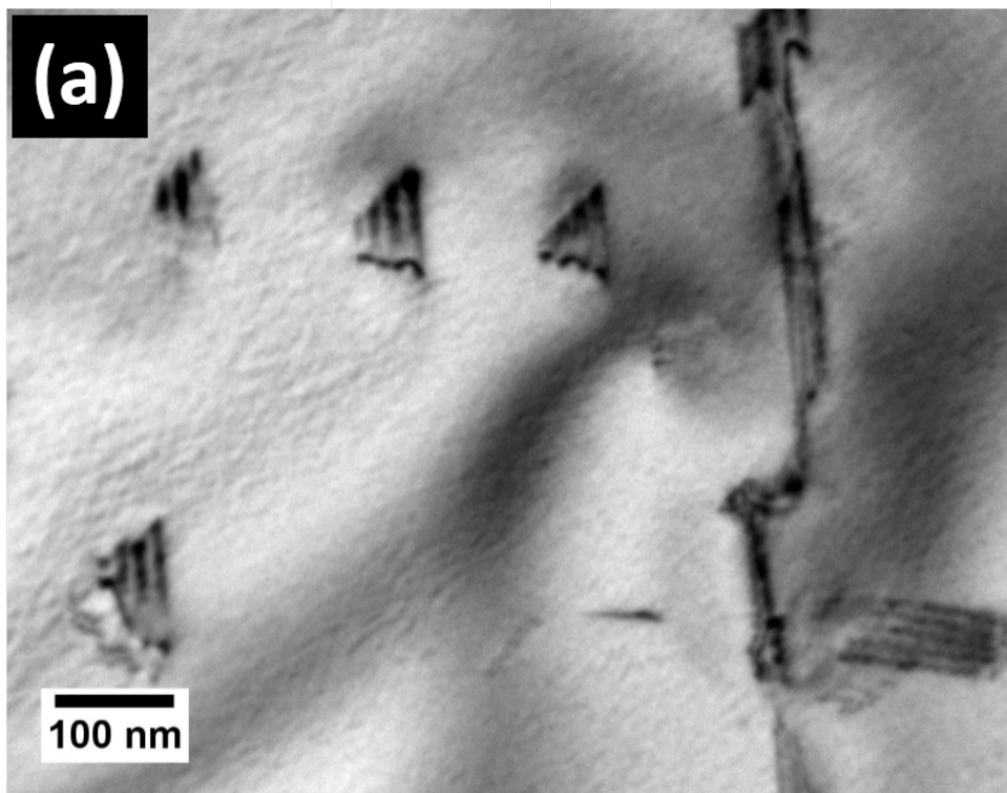
Fig. 13. SEM image surface fraction of γ , γ' , CoAl and Co_3W phases after 1000 h of ageing at 900°C and equilibrium volume fraction of phases at 900°C deduced from Kobayashi phase diagram.



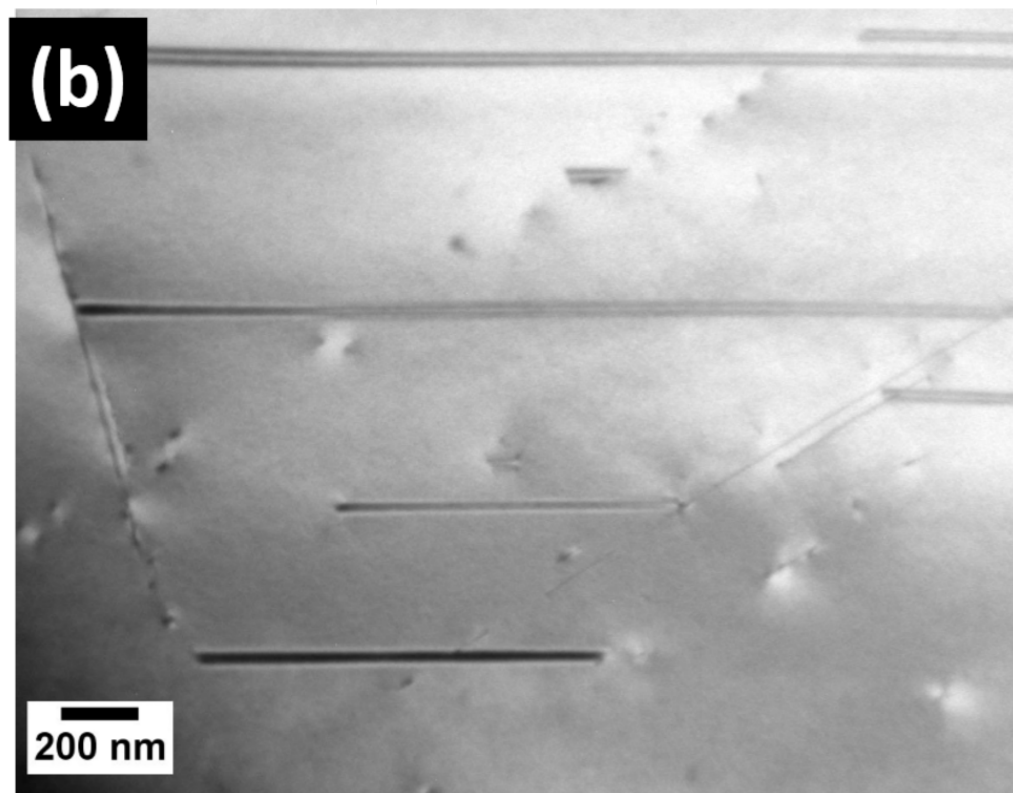




9Al7W

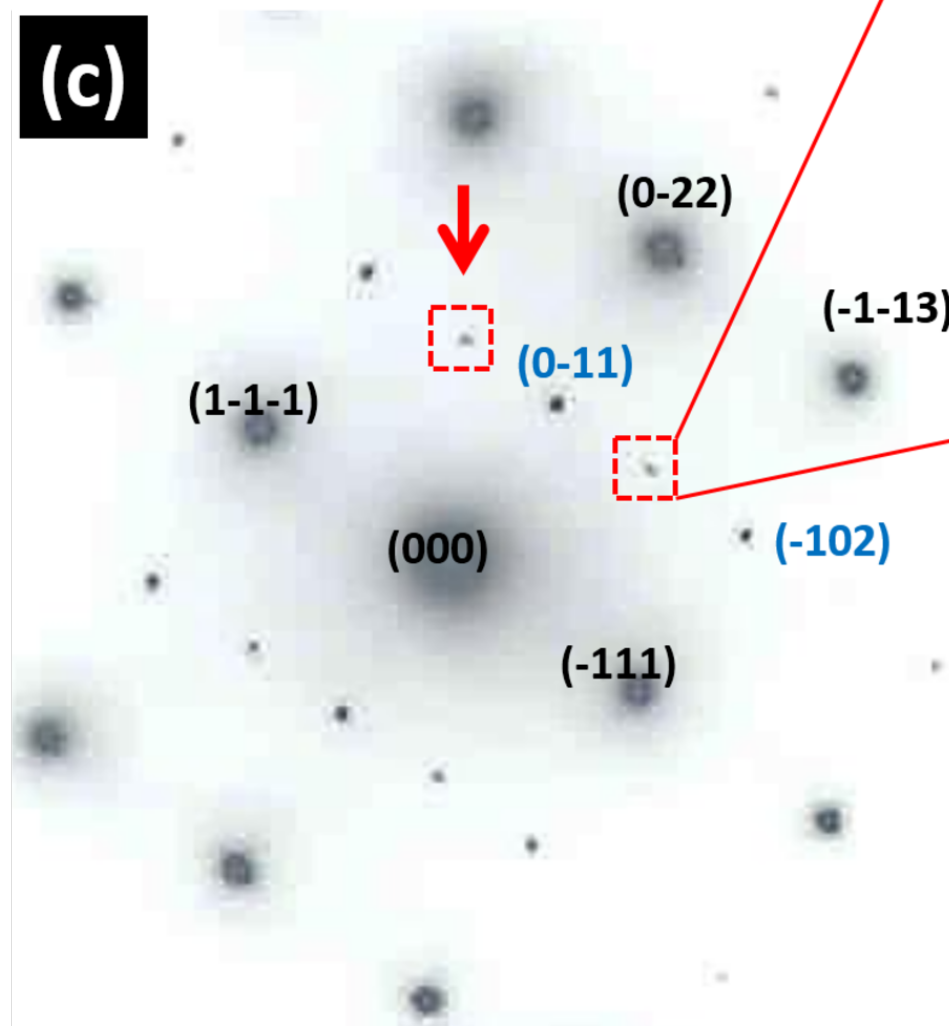


7Al9W

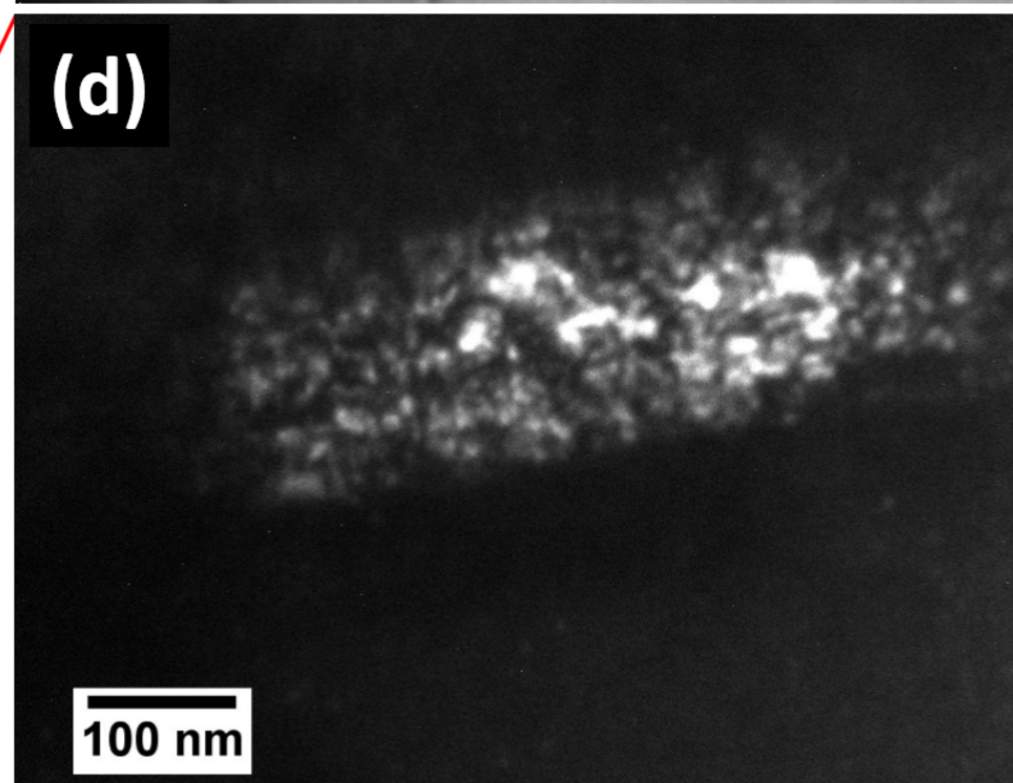


(c)

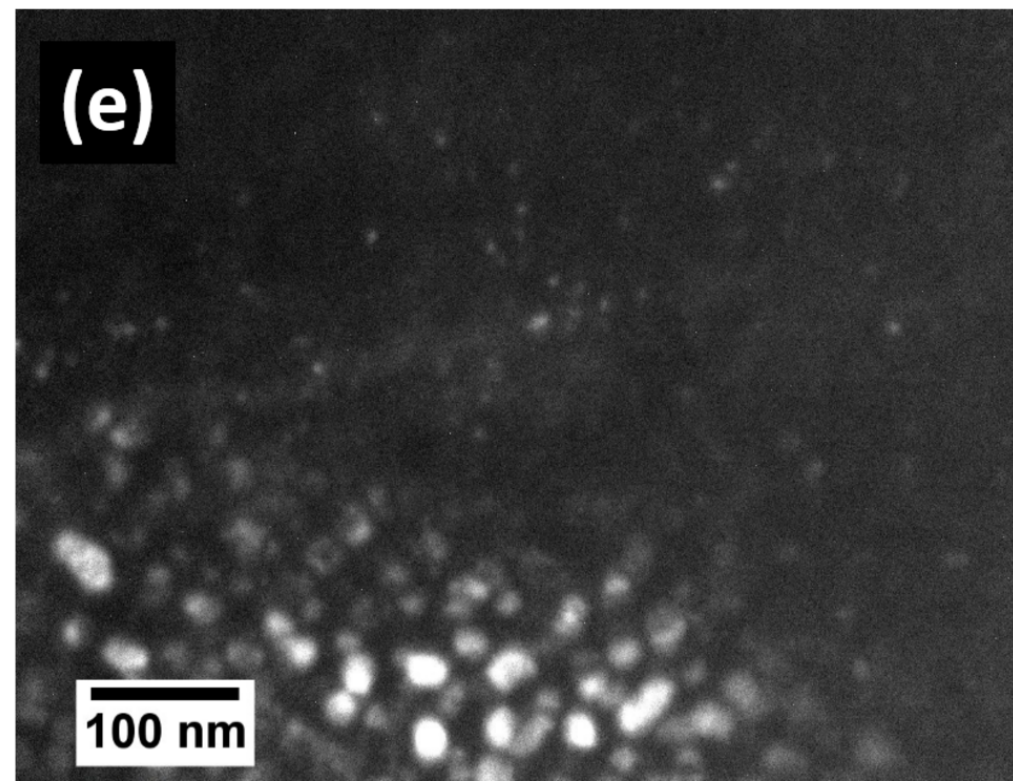
7Al9W

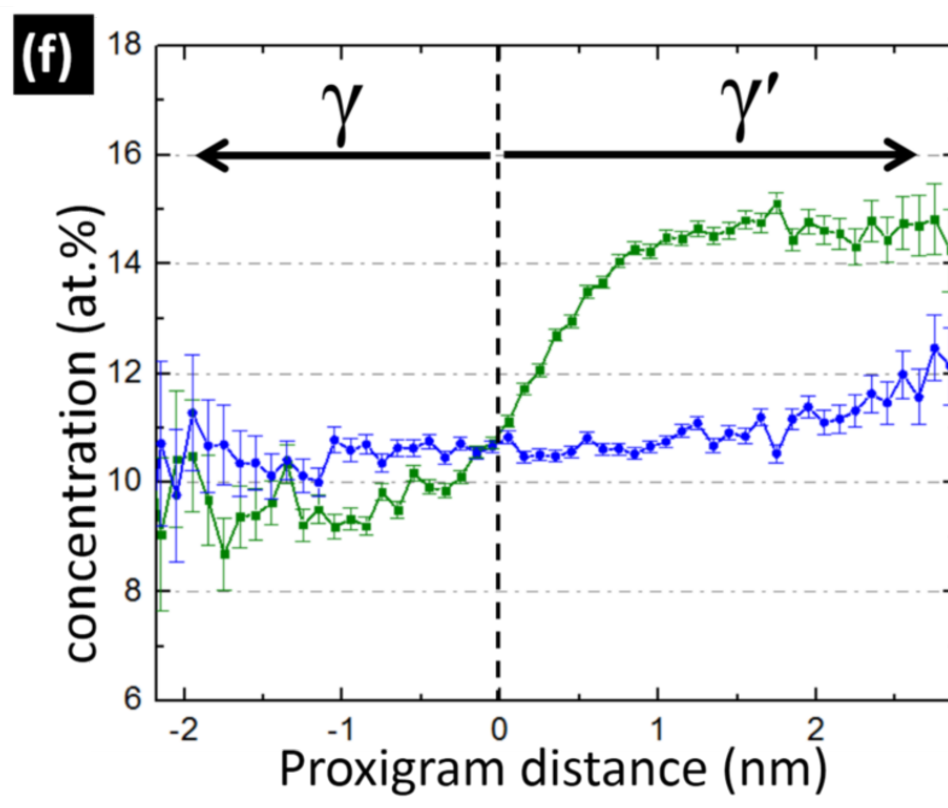
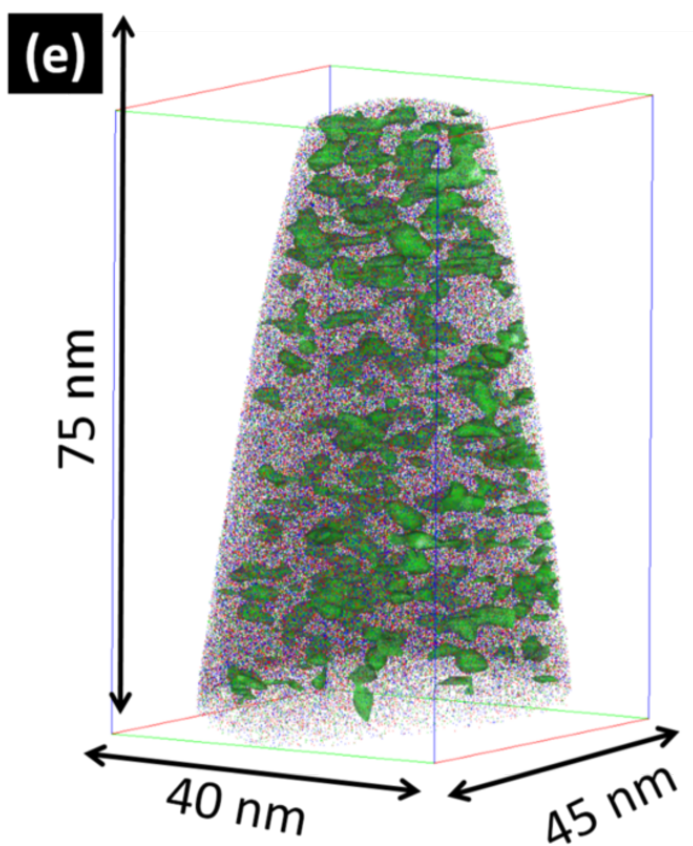
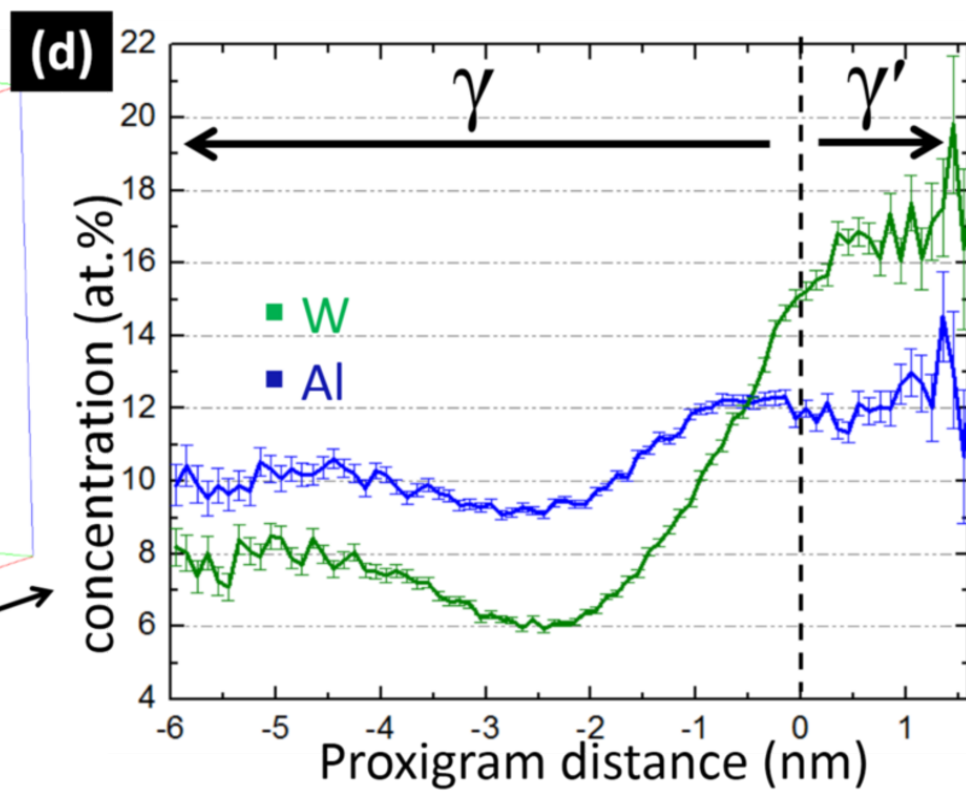
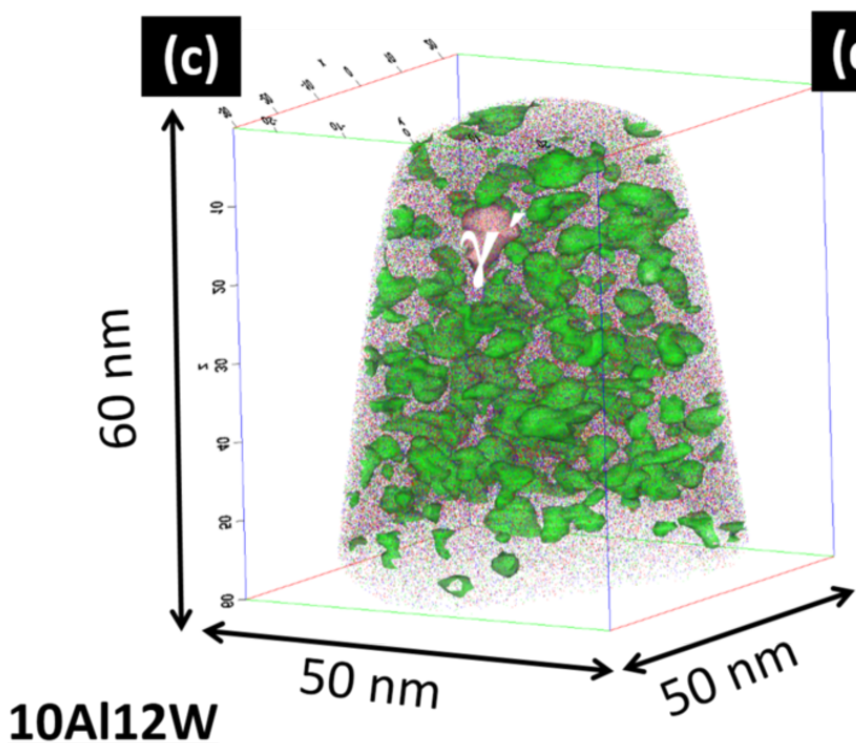
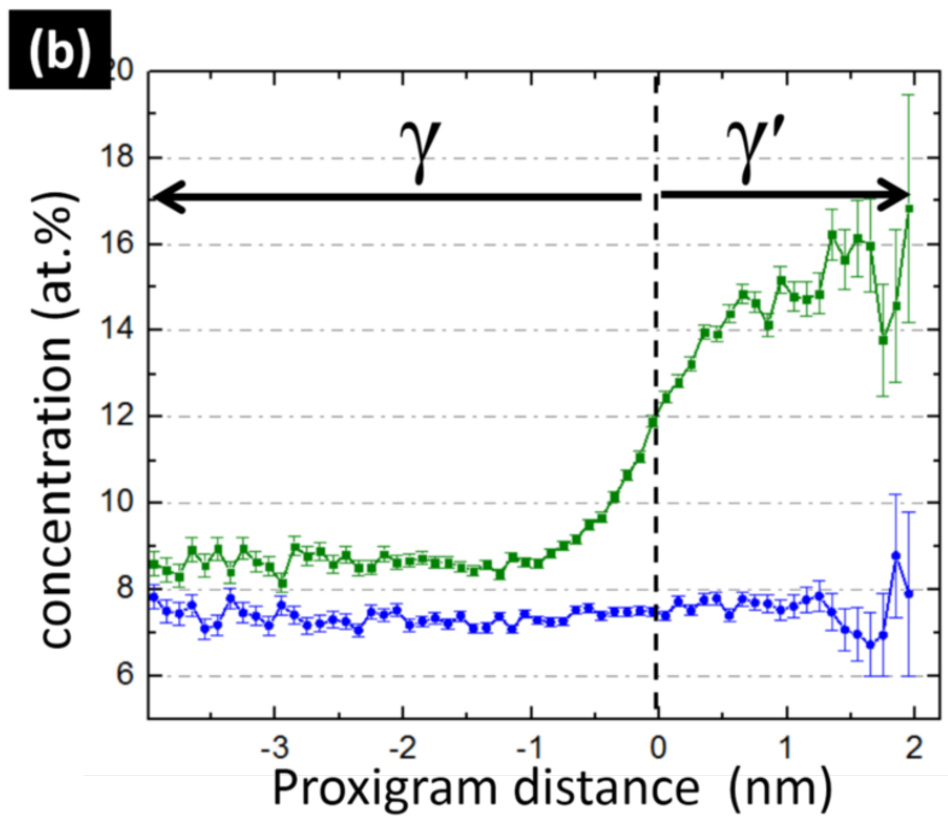
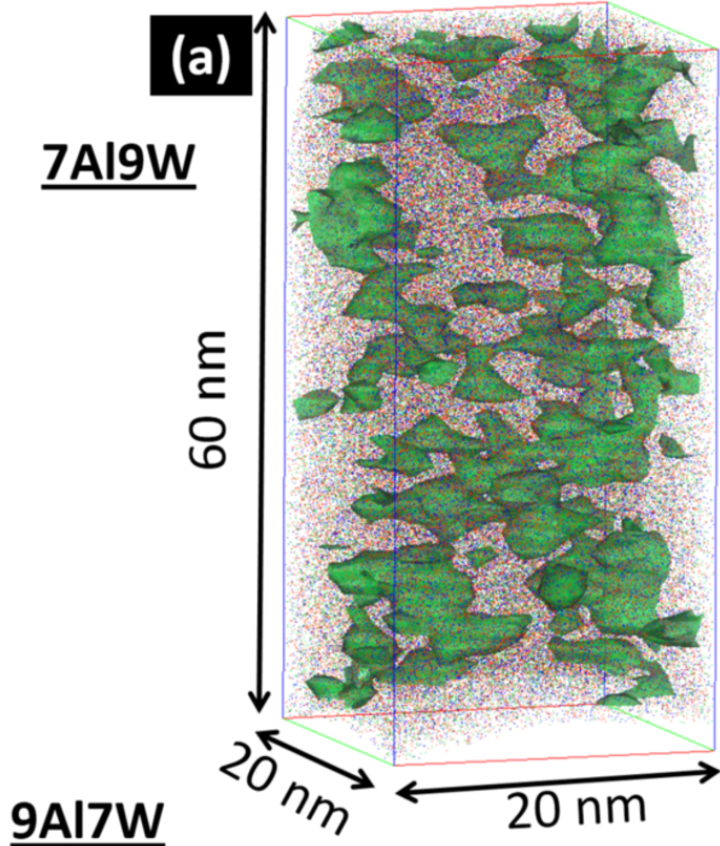


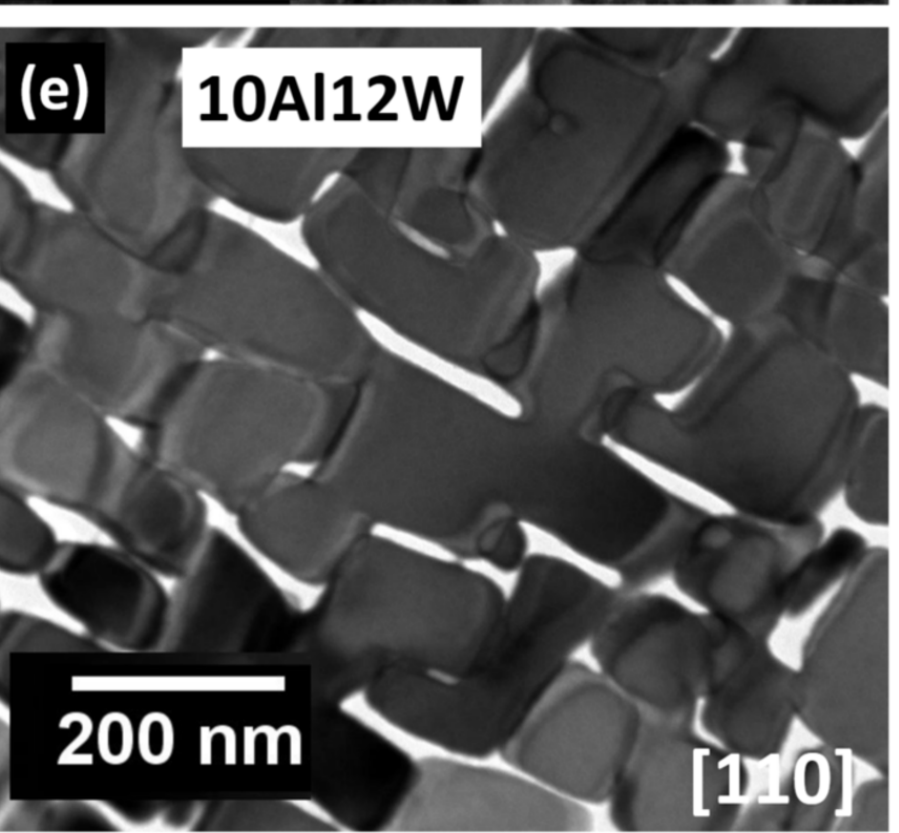
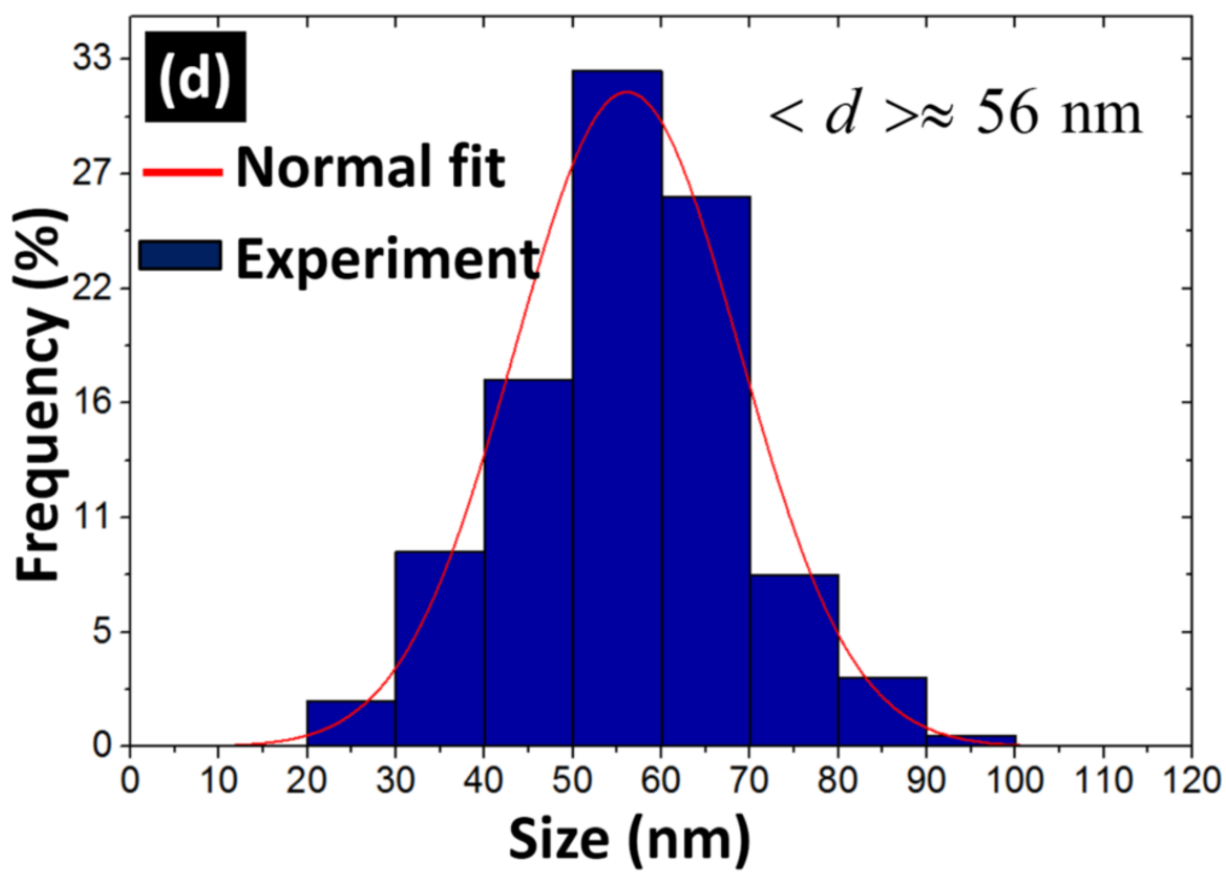
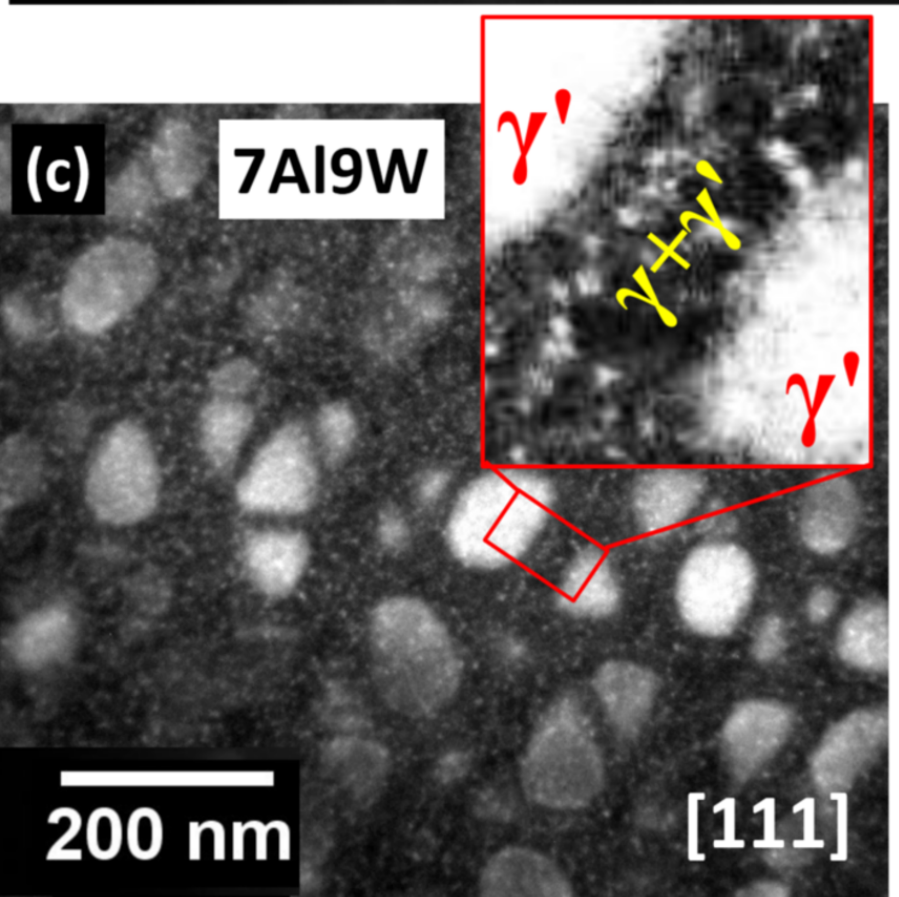
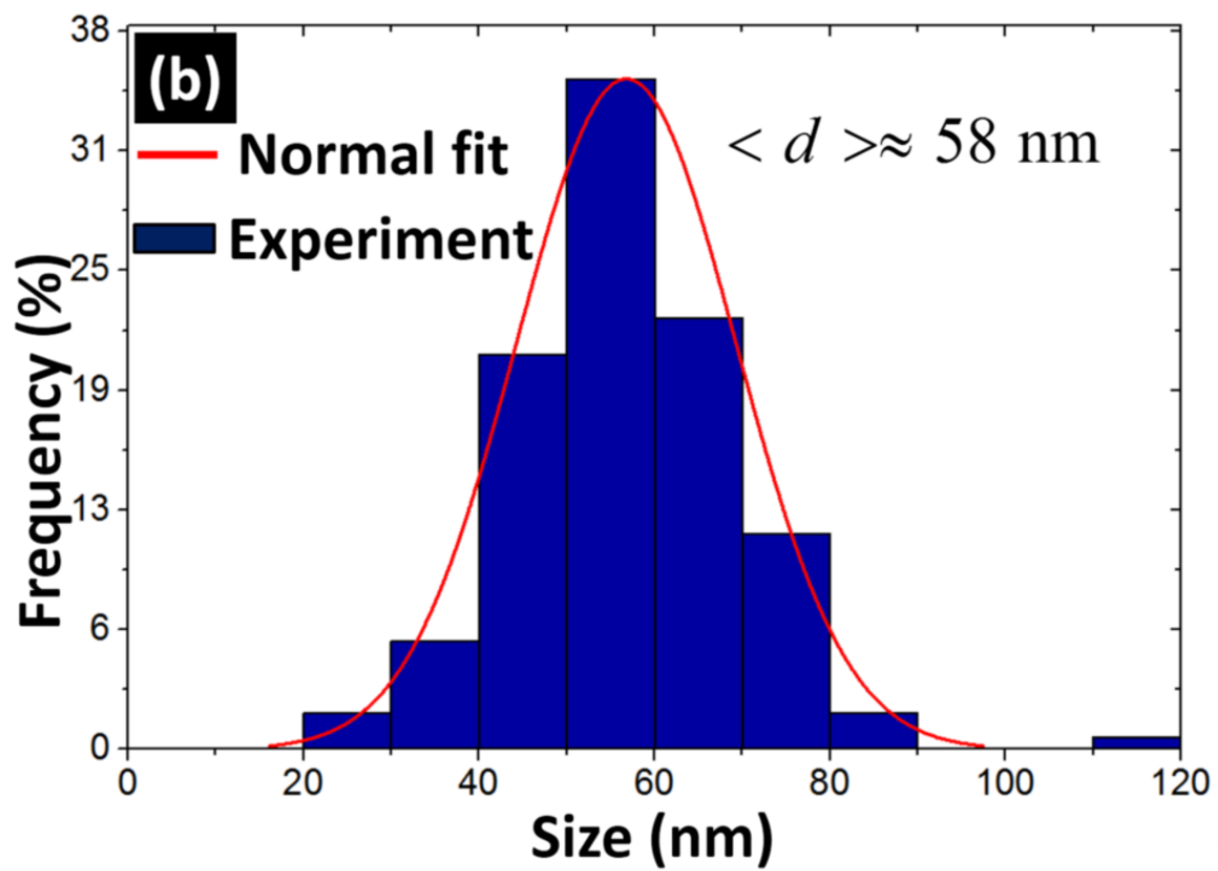
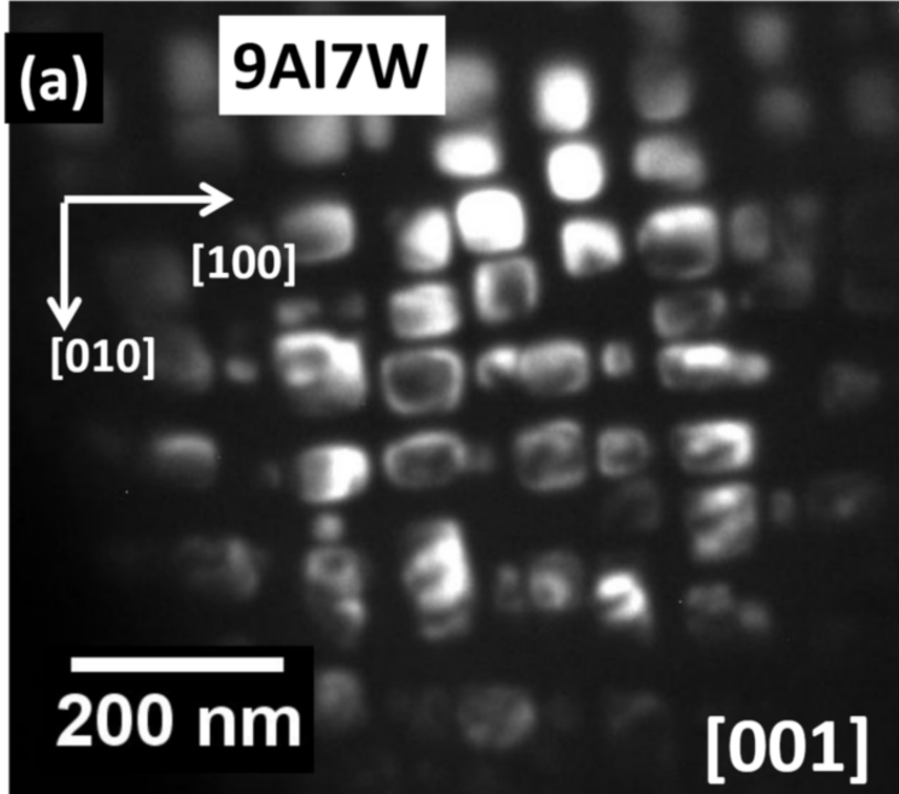
(d)

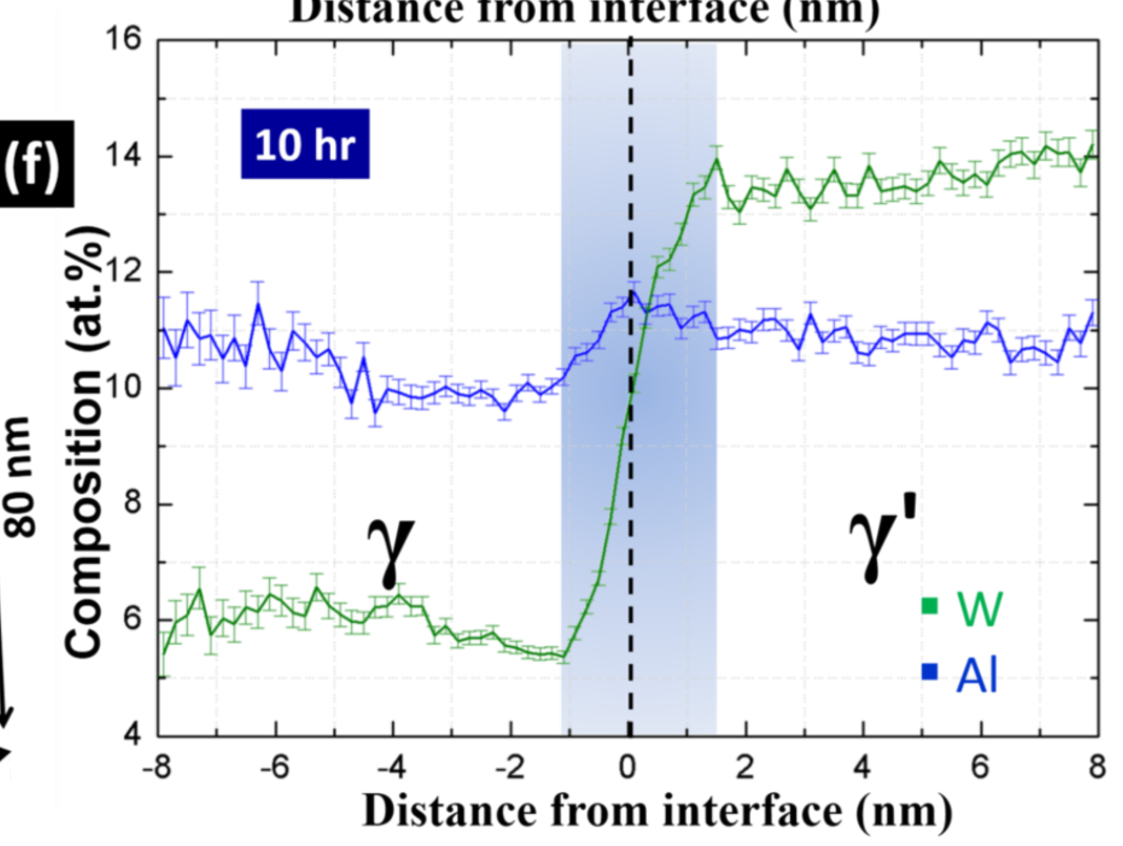
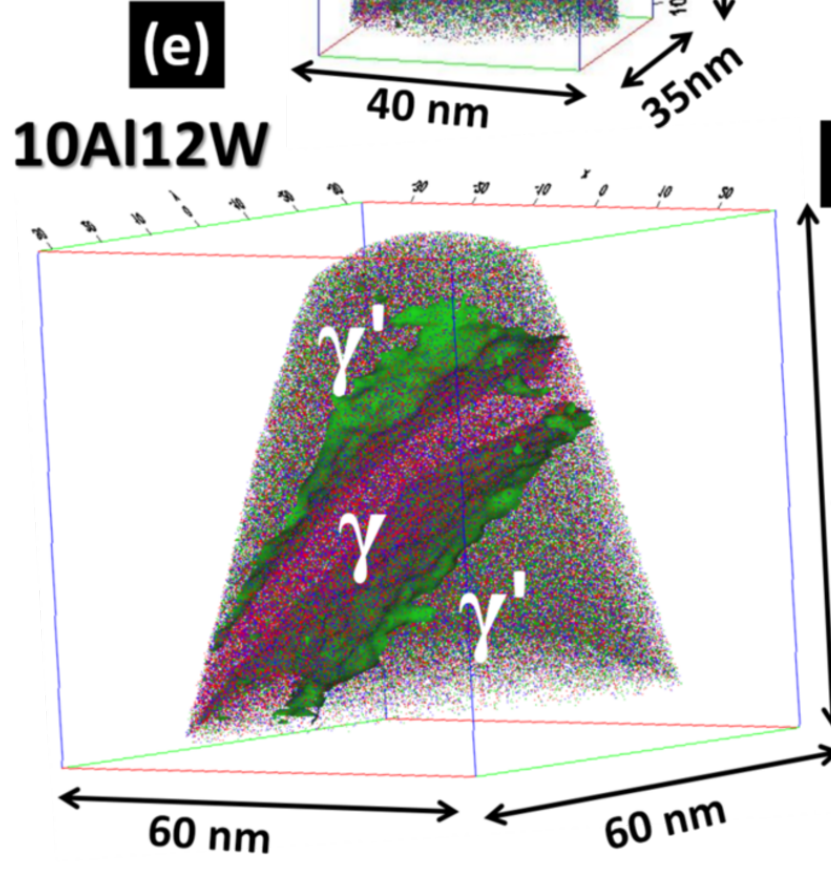
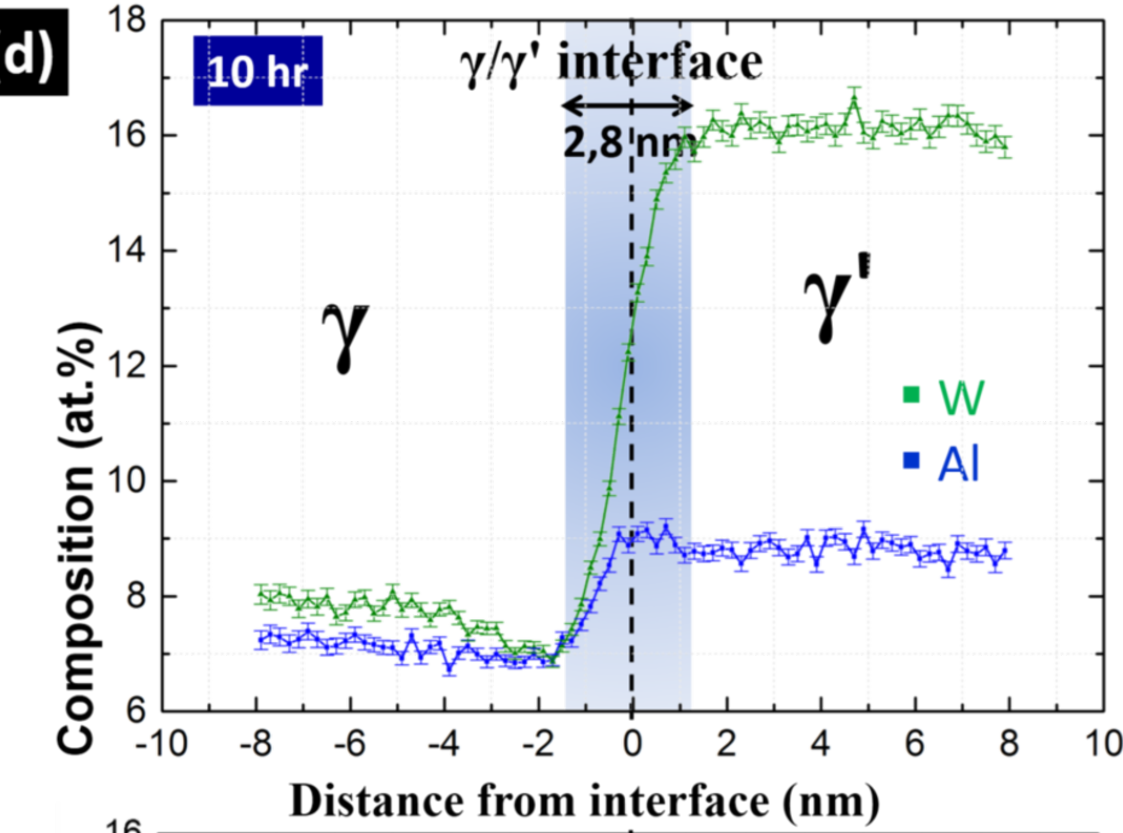
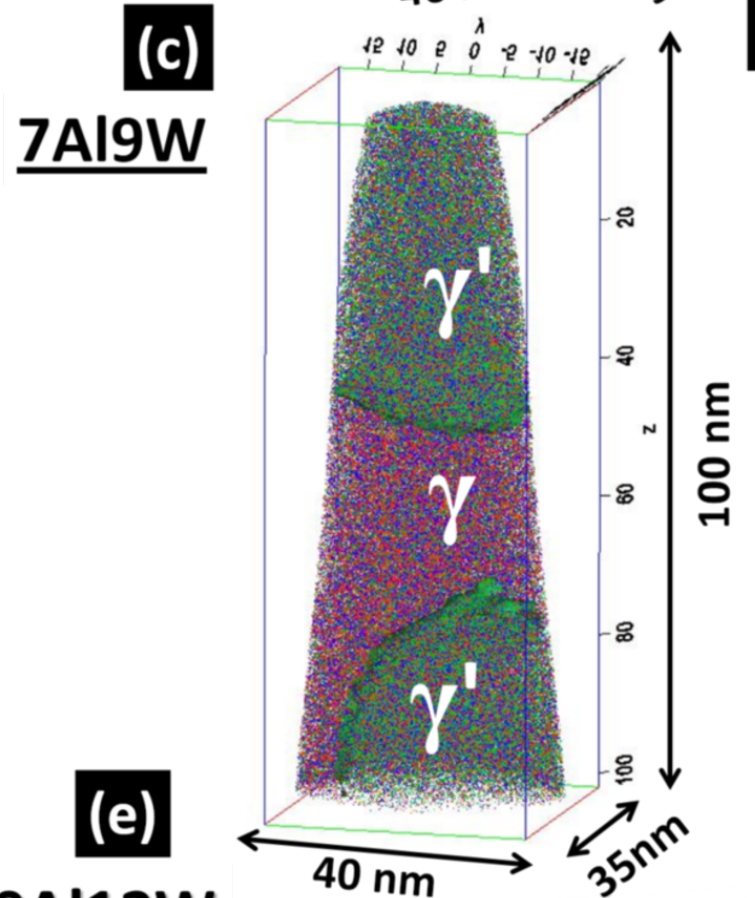
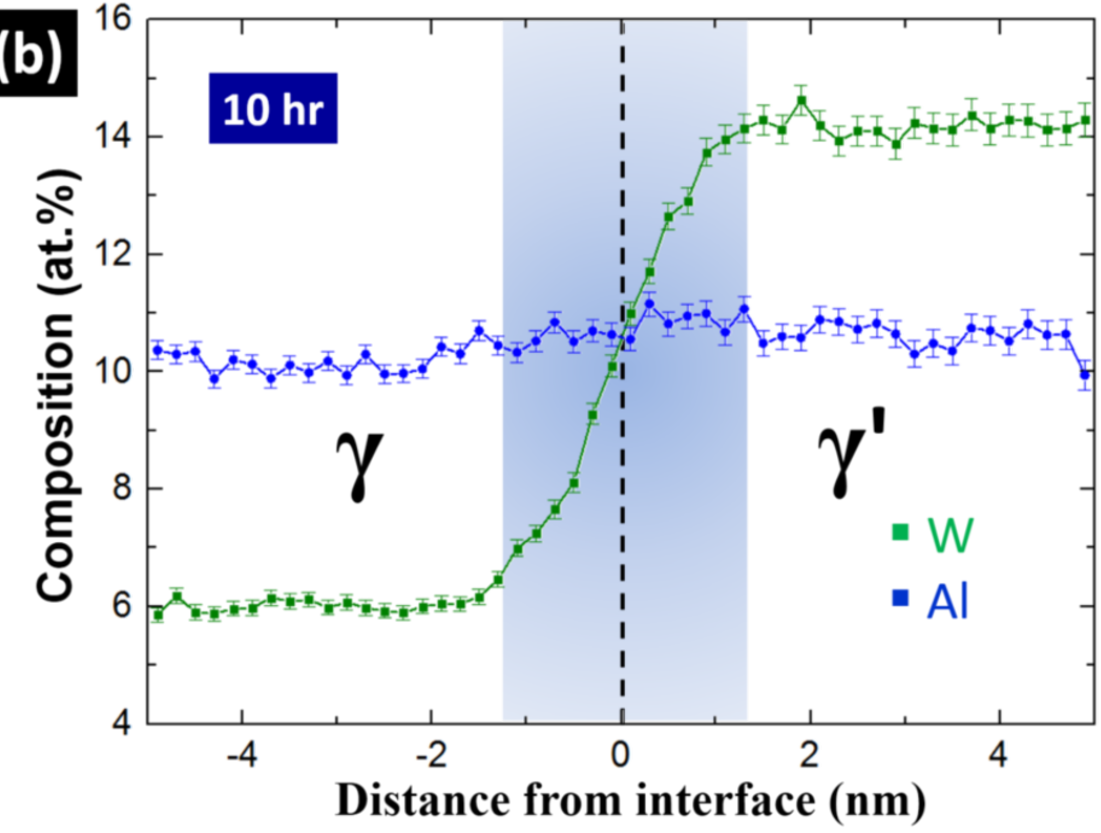
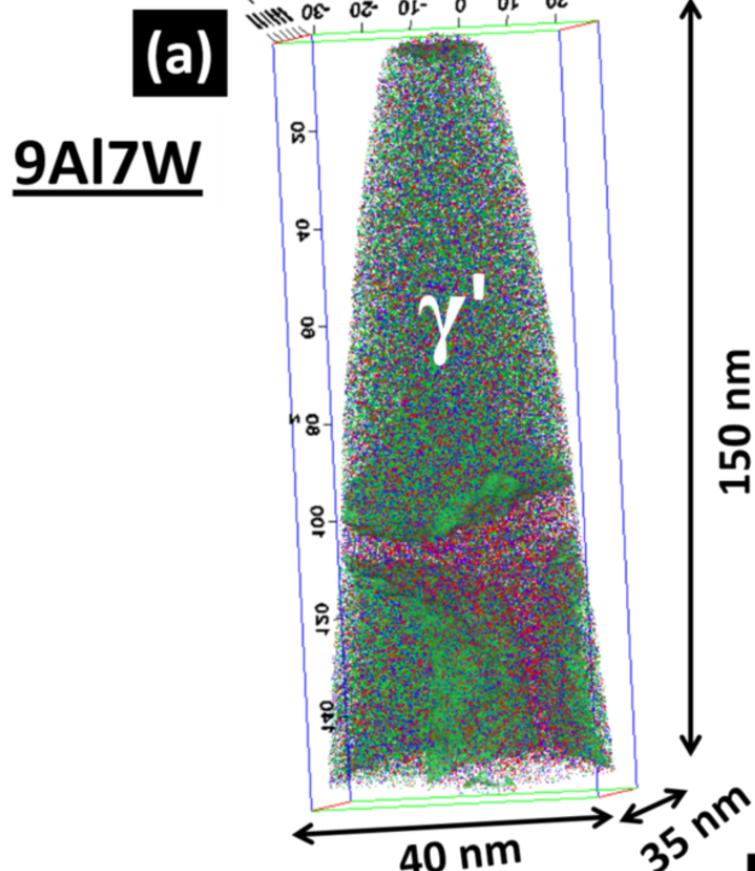


(e)

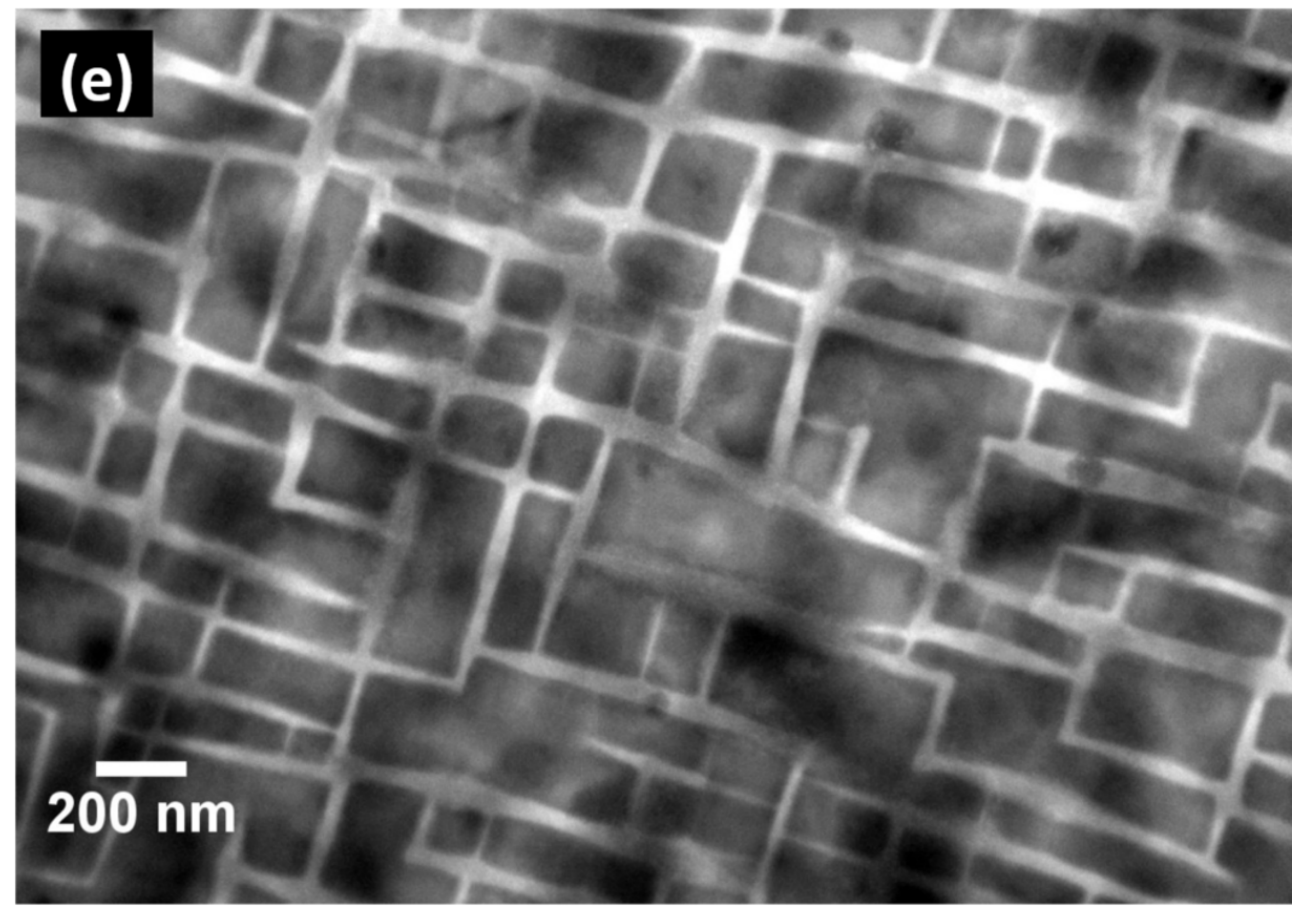
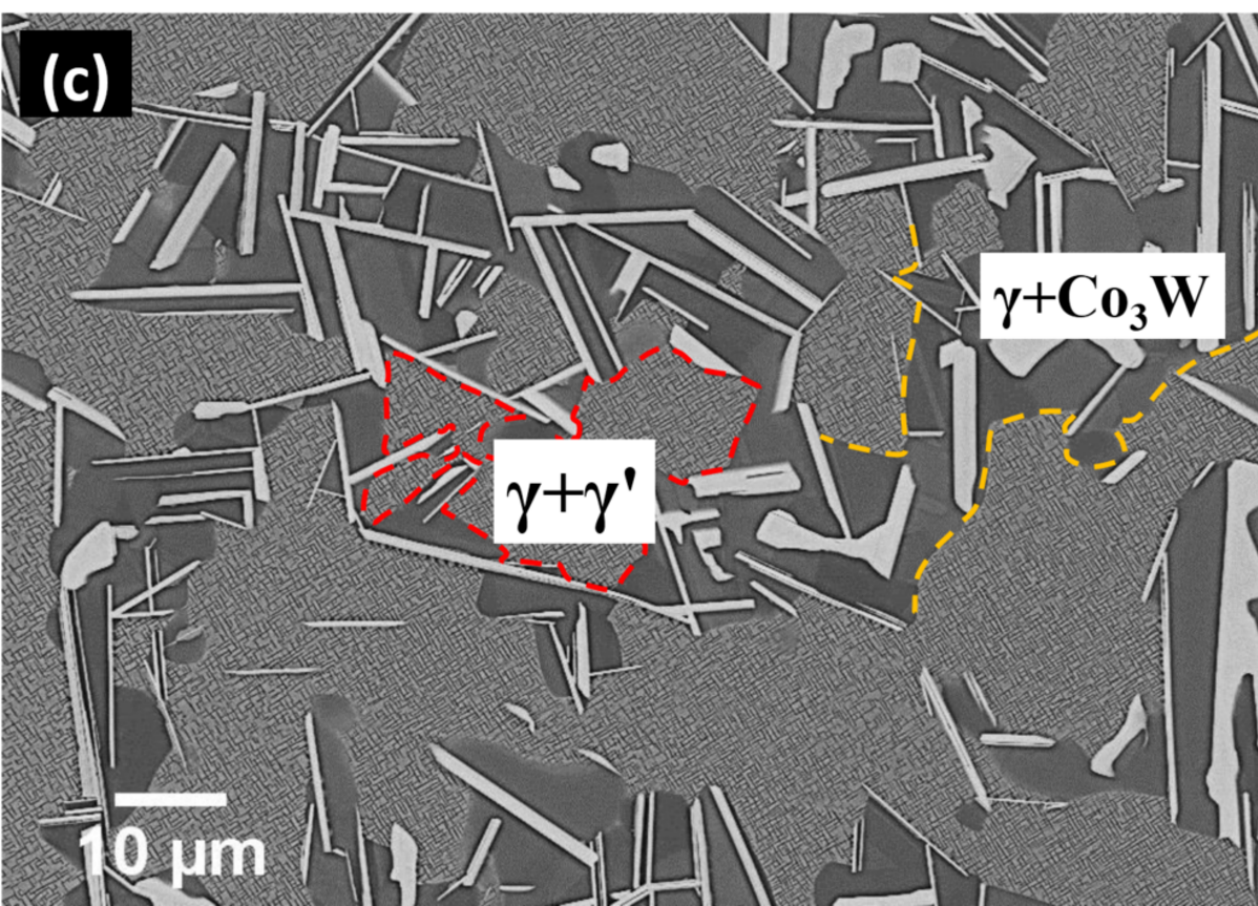
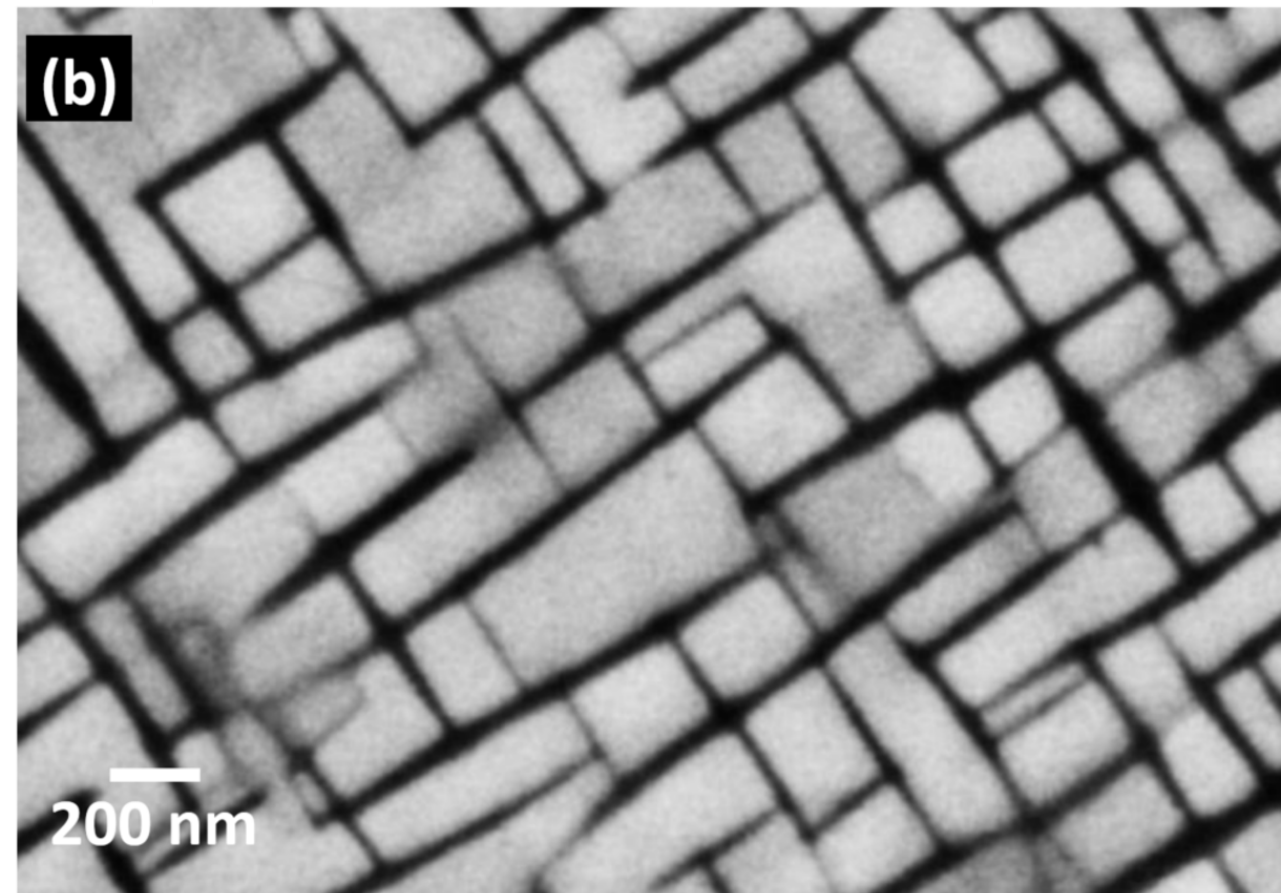
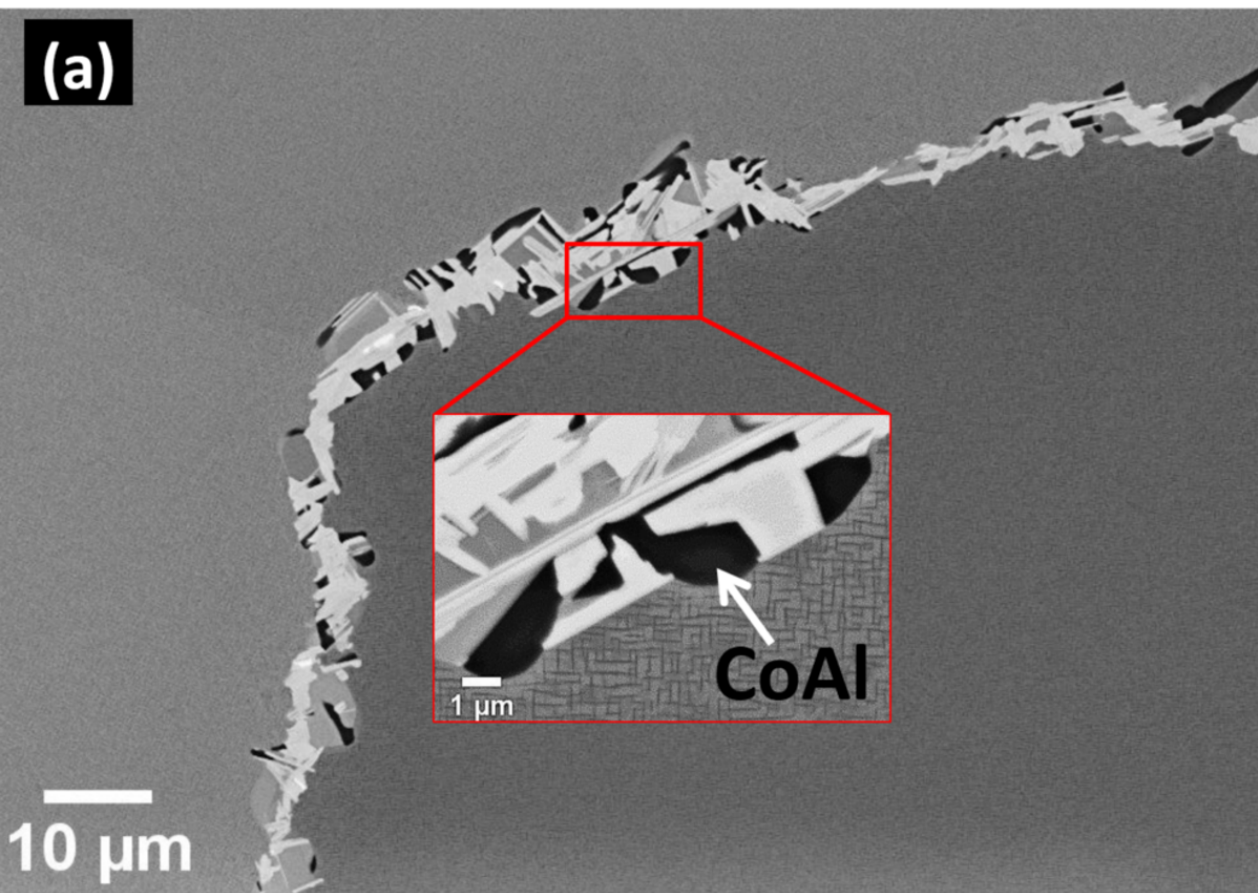




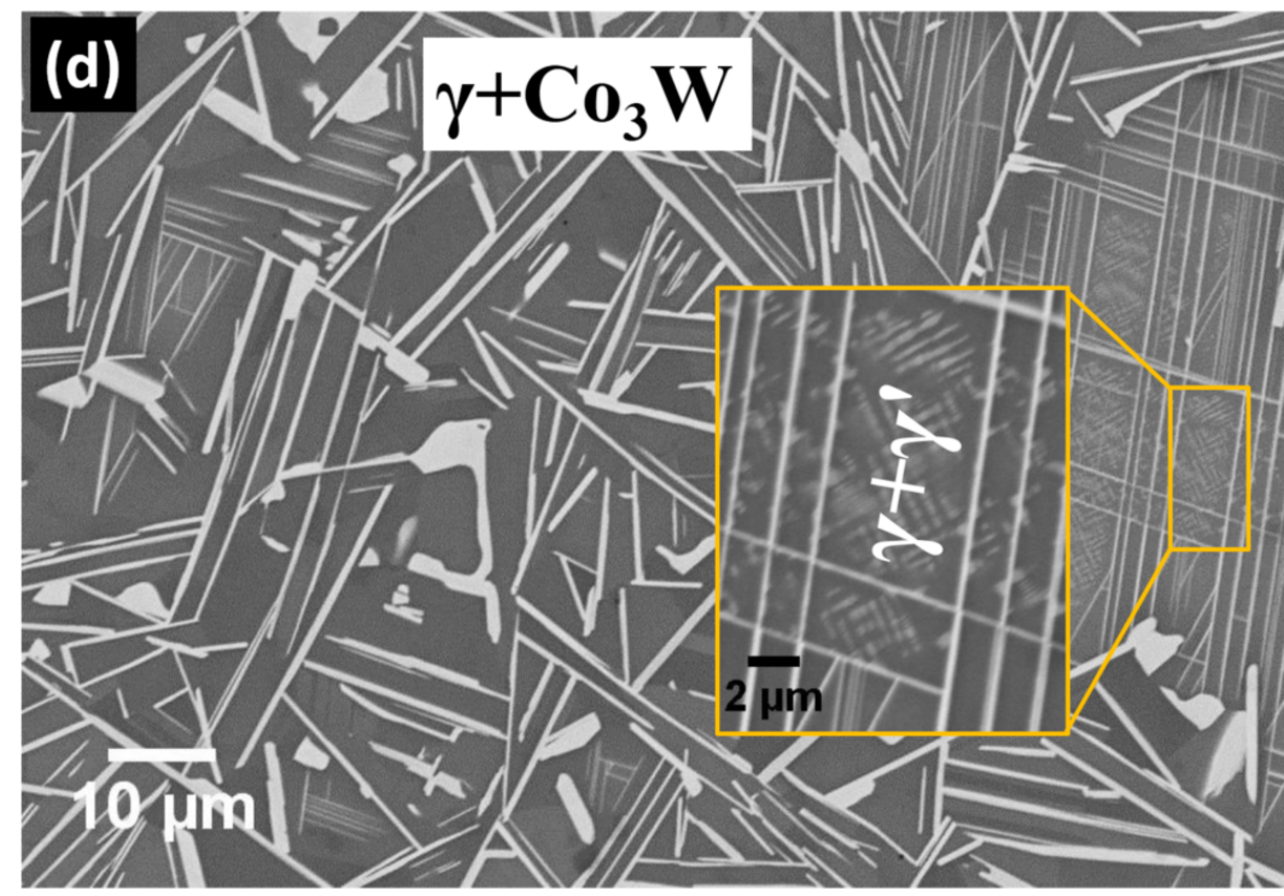
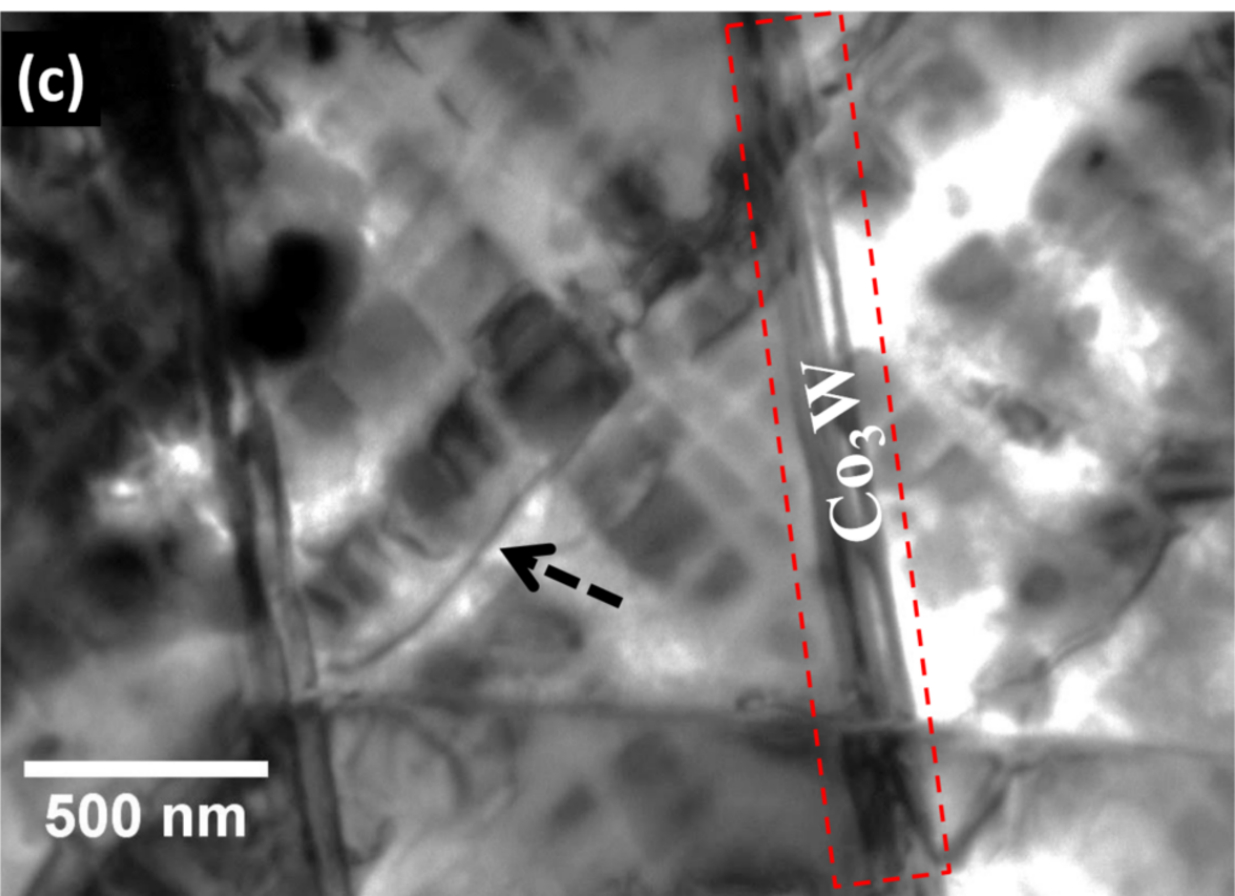
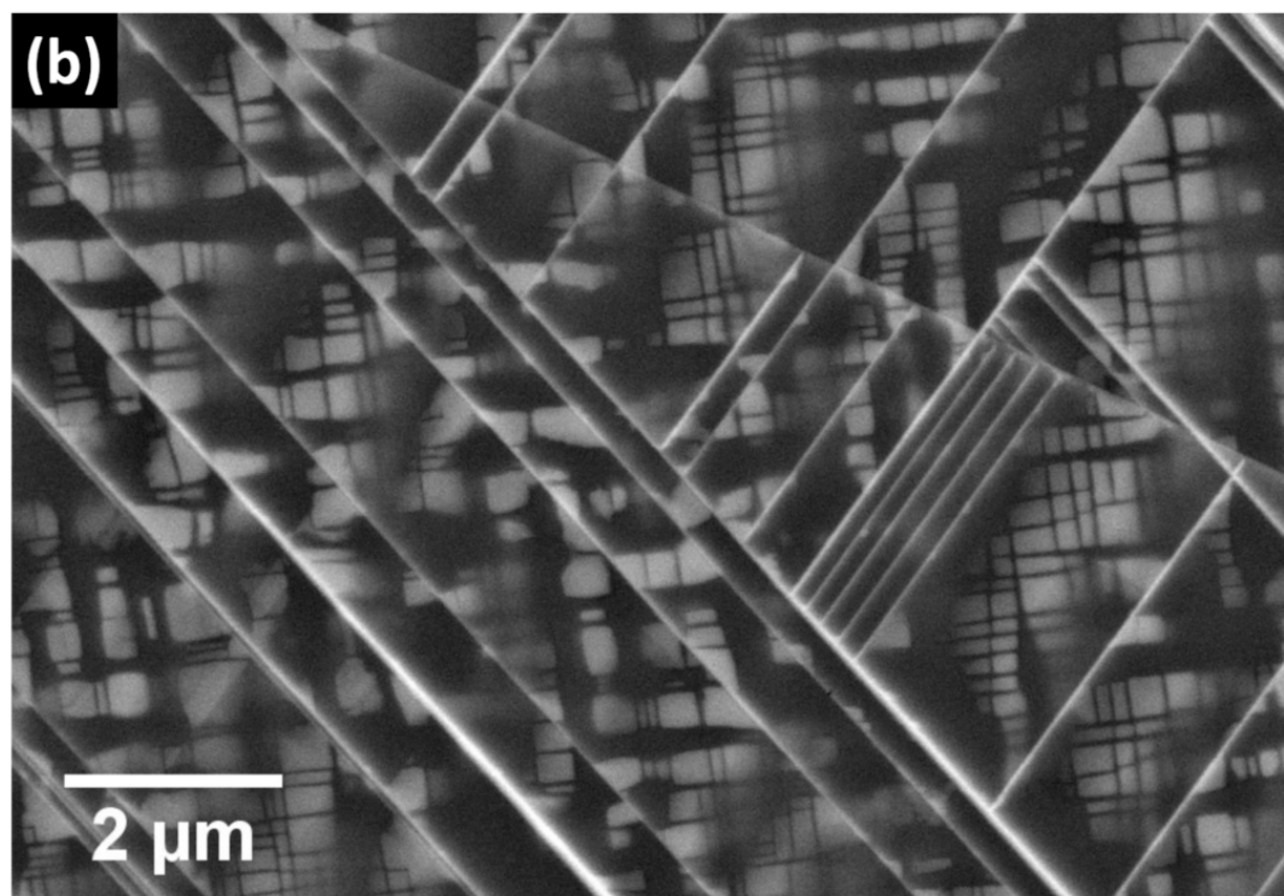
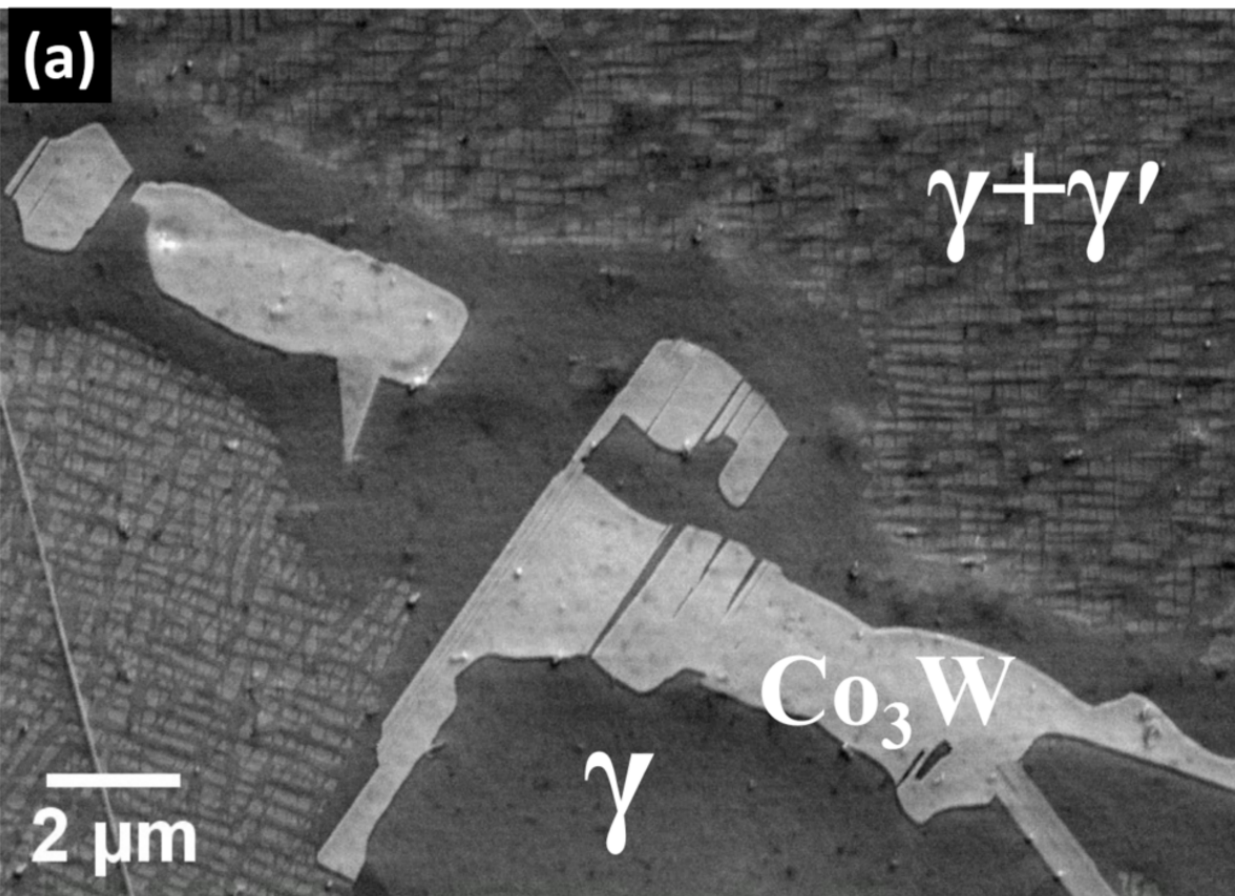




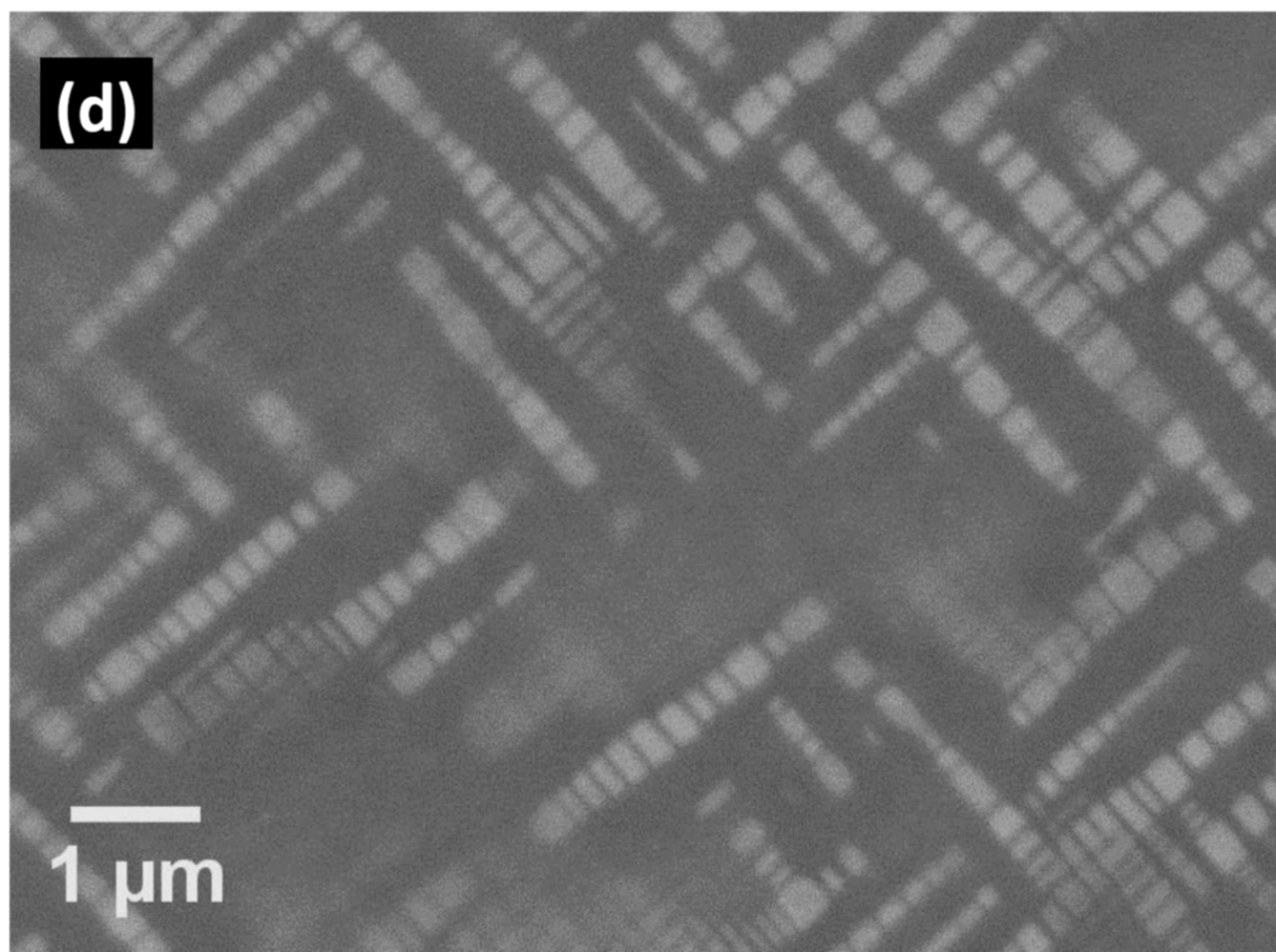
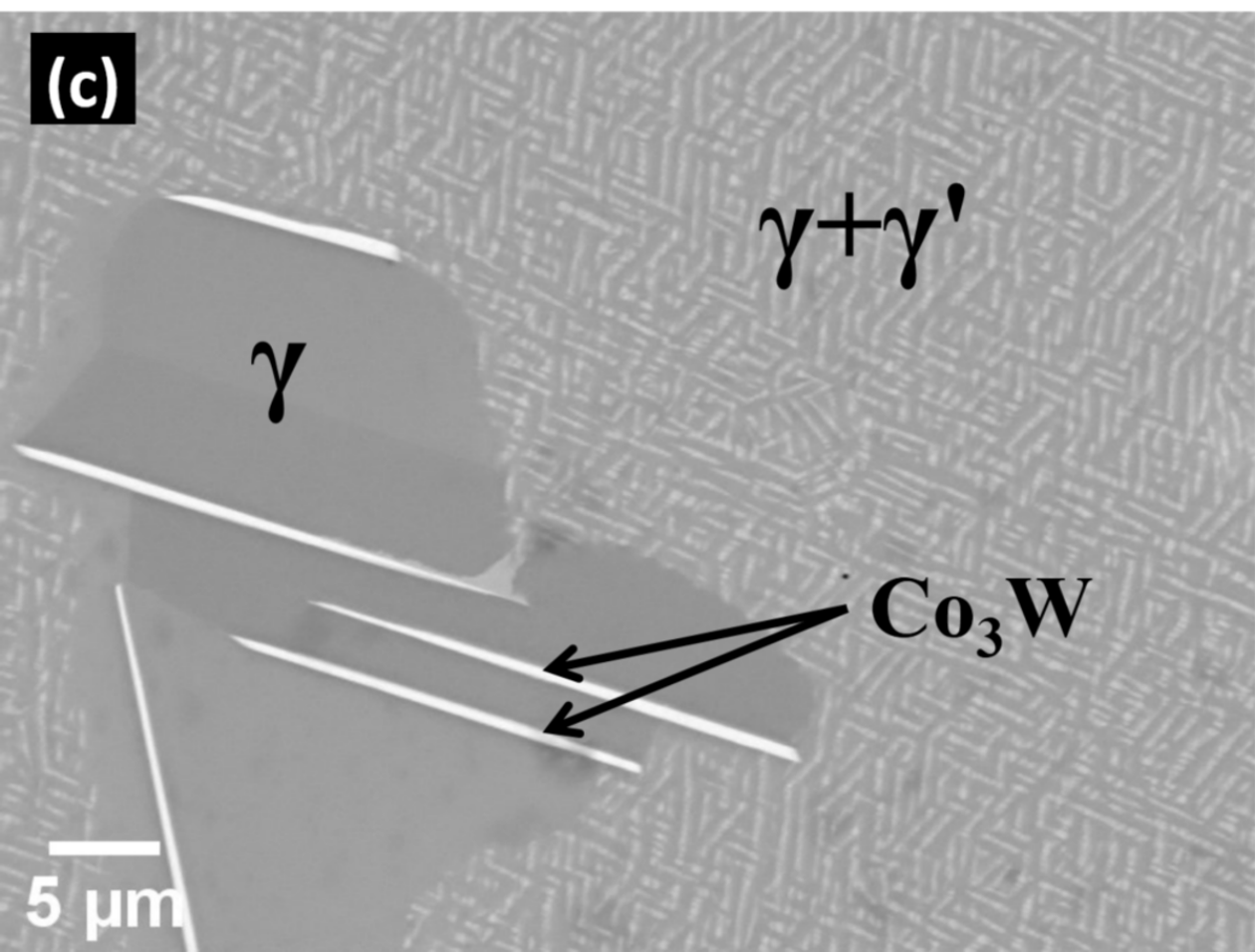
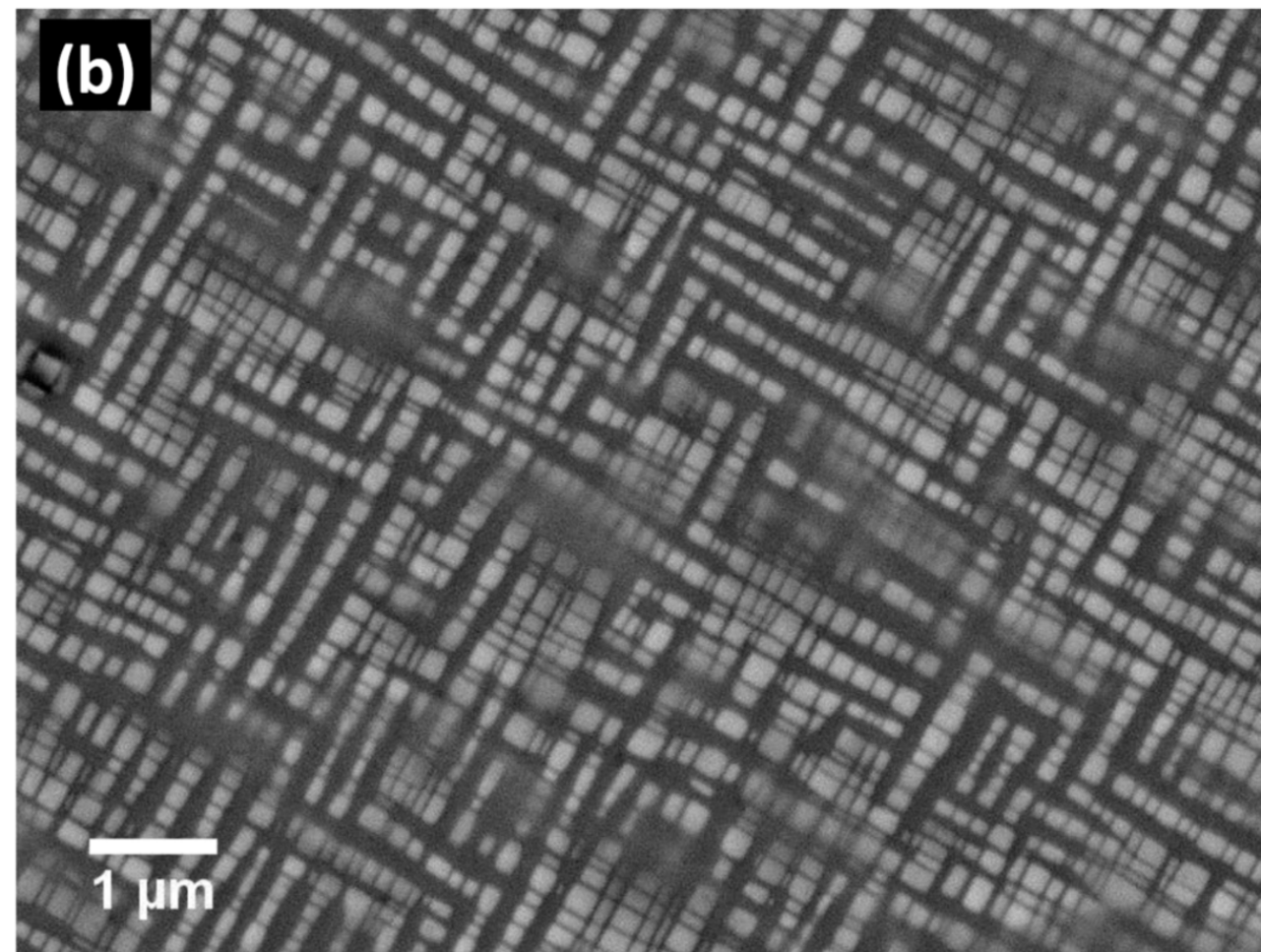
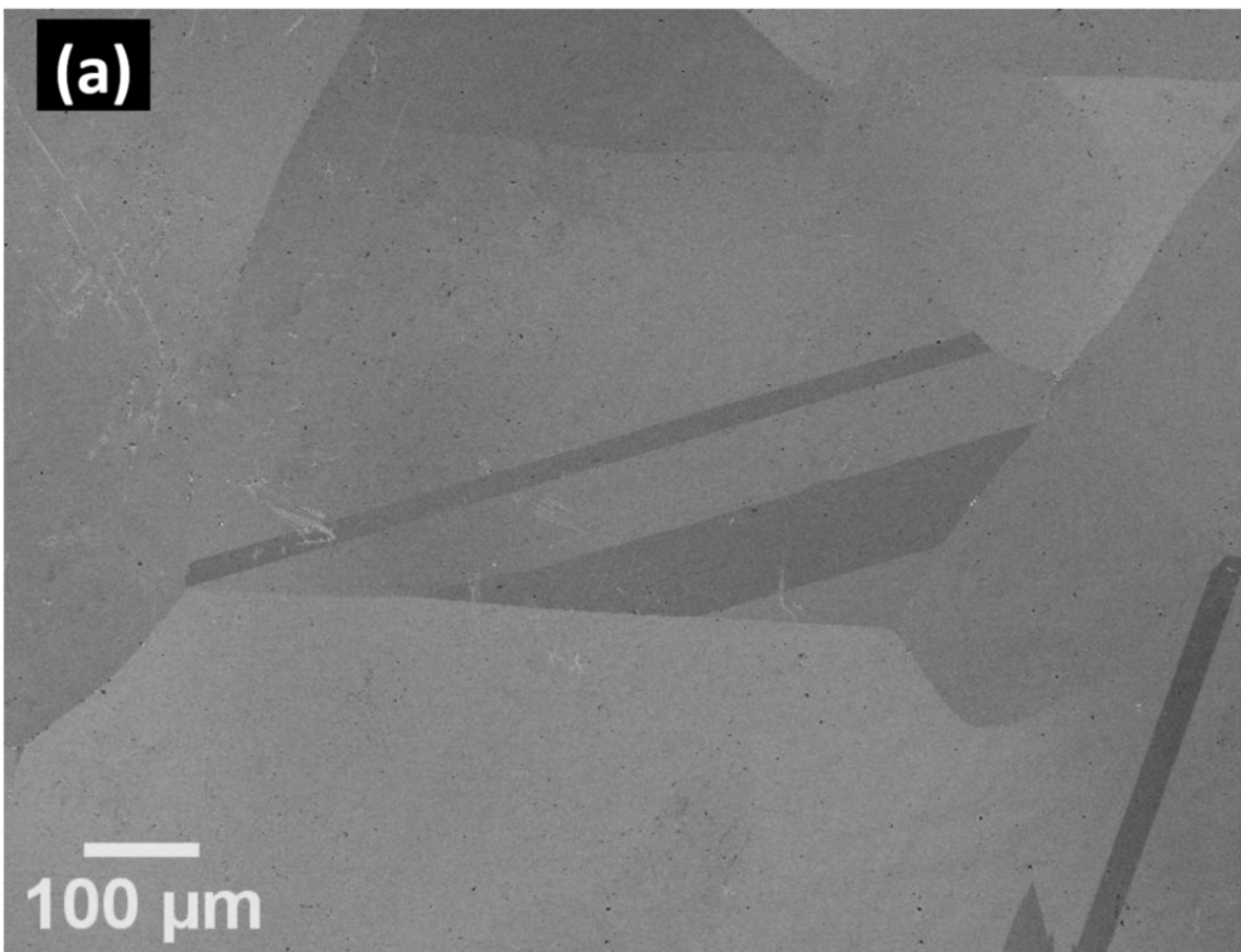
10Al12W



7Al9W



9Al7W



9Al7W

